

THE ROLE OF FIBROTIC SCAR FORMATION IN ISCHEMIC STROKE

Master Thesis

For the attainment of the academic degree

Master of Science

From the University of Applied Sciences FH Campus Wien

Submitted by:

LUCIJA PINTARIĆ

Personal identity code

c1810544021

Supervisor:

Dr. Richard Daneman
University of California San Diego
San Diego
United States of America

Submitted on:

18. 02. 2021

“It has been said, ‘time heals all wounds.’ I do not agree. The wounds remain. In time, the mind, protecting its sanity, covers them with scar tissue and the pain lessens. But it is never gone.”

- Rose Fitzgerald Kennedy

Abstract in English

Ischemic stroke is one of the leading causes of death and disability worldwide. However, since 1996 no new drugs have been approved to enhance the recovery from stroke. Following a stroke, glial and fibrotic scar formation occurs in and around the site of trauma. Glial scarring has been studied extensively throughout the years, but the role of the fibrotic scar in stroke recovery and the molecular mechanisms driving fibrosis has been overlooked. This research study has sought to answer these questions by determining the cells that are the main contributors of ECM deposition, the timecourse of fibrosis, and the role of fibrosis in motor recovery following cortical ischemia. We performed dMCAO on wild type C57BL/6 mice and found that there is robust fibrotic scarring found mainly in the lateral portions of the infarct core by day 14 and remains present on day 30. Single-cell sequencing on GFP+ cells isolated from infarct cortical tissue of Col1a1-GFP+ mice revealed that the cells responsible for ECM deposition and organization have a transcriptional profile of fibroblasts. Moreover, we used the HTK/GCV system to ablate dividing fibrotic scar forming cells and evaluate the rate of motor recovery by ATT, and demonstrated that the proliferation of scar-forming cells showed a neuroprotective phenotype at day 21 of recovery. These data delineate a framework for understanding the CNS fibrotic response. More experiments will be performed in the future to strengthen and validate these preliminary findings.

Abstract in German

Der ischämische Schlaganfall ist eine der häufigsten Ursachen für Tod und Behinderung weltweit. Es wurden jedoch seit 1996 keine neuen Medikamente zur Heilung von Schlaganfällen zugelassen. Nach einem Schlaganfall kommt es zur glialen und fibrotischen Narbenbildung in und um den Ort des Traumas. Die gliale Narbenbildung wurde in den letzten Jahren ausgiebig untersucht, aber die Rolle der fibrotischen Narbe in der Schlaganfall-Heilung und die molekularen Mechanismen, welche die Fibrose antreiben, wurden bisher übersehen. In dieser Studie haben wir versucht, diese Fragen zu beantworten, indem wir den zeitlichen Verlauf der Fibrose, die Zellen, die am meisten zur ECM-Ablagerung beitragen, und die Rolle der Fibrose bei der motorischen Heilung nach kortikaler Ischämie bestimmt haben. Wir führten dMCAO an Wildtyp-C57BL/6-Mäusen durch und fanden heraus, dass eine robuste fibrotische Vernarbung, die hauptsächlich in den lateralen Bereichen des Infarktkerns zu finden ist, an Tag 14 auftritt und an Tag 30 noch vorhanden ist. Die Einzelzellsequenzierung von GFP+-Zellen, die aus dem kortikalen Infarktgewebe von Col1a1-GFP+-Mäusen isoliert wurden, ergab, dass die Zellen, die für die Ablagerung und Organisation der ECM verantwortlich sind, ein Transkriptionsprofil von Fibroblasten aufweisen. Darüber hinaus verwendeten wir das HTK/GCV-System, um sich teilende fibrotische, narbenbildende Zellen abzutragen und die Rate der motorischen Heilung mittels ATT zu bewerten und konnten zeigen, dass die Proliferation der narbenbildenden Zellen am Tag 21 der Heilung einen neuroprotektiven Phänotyp zeigte. Diese Daten skizzieren einen Rahmen für das Verständnis der fibrotischen Reaktion des ZNS. Weitere Experimente werden in einem zukünftigen Projekt durchgeführt, um diese vorläufigen Ergebnisse zu bestätigen und zu festigen.

Table of Content

	Page
Abstract in English.....	3
Abstract in German.....	4
List of Figures, Tables and Illustrations.....	7
List of Abbreviations	9
1. Introduction.....	12
1.1 Fibrosis in Solid Organs.....	12
1.1.1 Mediators of Fibrosis.....	13
1.1.2 Sources and Role of Myofibroblasts.....	15
1.1.3 Extracellular Matrix Scaffolding.....	16
1.2 Stroke – Types and Causes.....	19
1.2.1 Ischemic Stroke – Ischemic Cascade and Phases of Recovery.	20
1.2.2 Therapeutic options for Ischemic Stroke.....	23
1.3 Fibrosis in the CNS.....	24
1.3.1 Astroglial and Fibrotic Scarring in Ischemic Stroke.....	26
1.4 Aims and Problem Statement.....	28
2. Materials and Methods.....	30
2.1 Experimental model and Subject details.....	30
2.2 Distal Middle Cerebral Artery Occlusion + 60 minute microvascular clamping.....	31
2.3 Tissue Processing.....	33
2.3.1 Whole animal Perfusion fixation and Drop fixation.....	33
2.3.2 Tissue slice collection.....	34
2.3.3 IHC staining.....	34
2.4 Adhesive Tape Test.....	36

	Page
2.5 scRNA sequencing experiment.....	38
2.5.1 Tissue Dissociation and FACS sorting	38
2.5.2 Single Cell RNA sequencing.....	39
3. Results.....	40
3.1 Timecourse of Fibrosis and Neuroinflammation in Stroke.....	40
3.1.1 Characterization of the Infarcts	40
3.1.2 Changes of the Infarct Core and Immediate Penumbra Region by Evaluation of Astrogliosis post ischemia.....	43
3.1.3 Fibrotic Response Evaluation by Col3 and ERTR7 IHC Through a Timecourse of 30 Days.....	45
3.1.4 Preliminary Neuroinflammatory Response Evaluation by CD45 and IBA-1 IHC Through a Timecourse of 30 Days.....	47
3.2 Single Cell RNA sequencing.....	50
3.2.1 FACS of GFP+ cells found within an ischemic infarct.....	50
3.3.2 Transcriptional profile of scar forming cells post MCAO.....	51
3.3 Recovery Implications of Fibrotic scarring.....	61
4. Discussion/Outlook.....	64
4.1 Conclusion.....	72
5. Literature.....	74
6. Acknowledgments.....	80
7. Statutory Declaration.....	82

List of Figures, Tables and Illustrations

	Page
Figure 1. A diagram representative of the different factors that mediate fibrosis formation.....	13
Figure 2. Major extracellular matrix components and their interactions with each other and cell membrane post cutaneous injury....	17
Figure 3. Simplified schematic overview of the pathophysiological mechanisms in the focally ischemic brain.....	21
Figure 4. Timecourse of the damaging event cascades in focal cerebral ischemia.....	22
Figure 5. Schematic depiction of the astroglial scar surrounding the infarct core following ischemic stroke and the subsequent cellular and molecular interactions in scar formation.....	27
Figure 6. Schematic depiction of distal middle cerebral artery perfusion in combination with 60-minute clamping time.....	32
Figure 7. Characterization of infarcts by evaluation of cortical regionality, total brain volume affected and hemisphere asymmetry.....	41
Figure 8. Infarct Core quantification defined by GFAP+ cellular margin and depiction of morphological changes of astrocytes.....	44
Figure 9. Collagen 3 and ERTR7 showing fibrotic scar formation in wt C57bl/6 mice in a period of 30 days post-ischemia.....	46

	Page
Figure 10. Neuroinflammatory response evaluated by IF of CD45 and Iba-1 wt C57bl/6 mice in a period of 30 days post-ischemia and the respective controls.....	48
Figure 11. Flow cytometry analysis of live Col1GFP+ cells in the ischemic cortex of day 14 mice after permanent distal middle cerebral artery occlusion.....	50
Figure 12. (A-I) Scar-forming cells have the transcriptional profile of fibroblasts at the single cell level and (G-I) the respective violin plots of the expression levels of pericyte, vSMC and fibroblast- specific genes per cluster.....	53
Figure 13. Heat map of the expression levels of the top 61 differentially expressed genes by Col1a1GFP+ cells from 7- and 14-days post dMCAO and Col1a1GFP+ cells from health.....	57
Figure 14. Adhesive Tape Test evaluation of limb function post stroke.....	62
Table 1 25 most relevant pathways that are implicated with genes upregulated in MCAO fibroblasts isolated by scRNAseq, sorted by p-value and determined by Reactome.....	59

List of Abbreviations

Abcc9 - ATP-binding cassette, sub-family C member 9

Acta2 - Actin Alpha 2, Smooth Muscle

Akt - Protein kinase B (also known as PKB)

ANG II - Angiotensin II

ANOVA - Analysis of Variance

ATT - Adhesive tape test

B6 - strain of mice, full name: B57bL/6J

BBB - Blood Brain Barrier

BSA - Bovine serum albumin

CCA - Common Carotid Artery

CD45/31 - Cluster of Differentiation 45/31

CDC - The Centers for Disease Control and Prevention

CNS - Central Nervous System

Col - Collagen

Cre - tyrosine recombinase enzyme

CTGF - connective tissue growth factor

CuSO₄ - copper sulphate

CV - Cresyl Violet

D-PBS - Dulbecco's phosphate-buffered saline

DAPI - 4',6-diamidino-2-phenylindole

dMCA - distal middle cerebral artery

dMCAO - distal middle cerebral artery occlusion

DNA - Deoxyribonucleic acid

DPX - Dibutylphthalate Polystyrene Xylene

EAE - Experimental autoimmune encephalomyelitis

ECM - Extracellular matrix

EGF - epidermal growth factor

EMT - epithelial-mesenchymal transition

EndMT - endothelial to mesenchymal transition

ERT - Estrogen Receptor

FACS - flow activated cell sorting

FAK1 - Focal adhesion kinase 1

FGF - fibroblast growth factor
Fn - Fibronectin
GAGs – glycosaminoglycans
GCV – Ganciclovir
GEMs - Gel Beads in Emulsion
GFP – Green Florescent Protein
HA - Hyaluronan
HSPGs - Heparan sulfate proteoglycans
HTK - herpes simplex virus thymidine kinase
IACUC - Institutional Animal Care and Use Committees
IBA-1 – ionized calcium binding adaptor molecule 1
IF – Immunofluorescence
IGF - insulin-like growth factor
IGFBP - Insulin-like growth factor binding protein
IHC – Immunohistochemistry
IL – Interleukin
IP – Interperitoneal
IPF - Idiopathic pulmonary fibrosis
Kjnc8 - Potassium Inwardly Rectifying Channel J8
KO - Knockout
LBP – LPS binding protein
LDL – Low density lipoprotein
Lmod1 - Leiomodin 1
MAP - mitogen-activated protein
MCA – middle cerebral artery
MCAO – middle cerebral artery occlusion
MCP-1 - monocyte chemoattractant protein-1
MMP – Matrix metalloproteases
Myh11 - Myosin Heavy Chain 11
NaCl – Sodium Chloride
NCAM1 - Neural Cell Adhesion Molecule 1
NDS – Non-specific Donkey Serum
NGS - Non-specific Goat Serum

NG2 - Neural/glial antigen
O/N - Overnight
OCT - Optimal Cutting Temperature Compound
PAMPS - Pathogen-associated molecular patterns
PBS - Phosphate-buffer solution
PDGF - Platelet-derived growth factor
PFA- Paraformaldehyde
PI3K - Phosphoinositide 3-kinase
PLD - Post lesion day
post-OP - Post operative
Postn - Periostin
PVM - Perivascular macrophages
RGS5 - Regulators of G protein signaling
RT - Room temperature
rTPa - Recombinant tissue plasminogen activator
SAP - acute phase proteins
scRNA - Single Cell RNA
SEM - Standard Error of Mean
Seq - Sequencing
SMA - Smooth muscle actin
SR/LAB - Sustained-Release for Laboratory Use in Rodents
STAIR - Stroke Therapy Academic Industry Roundtable
TBI - Traumatic brain injury
Timp1 - Metallopeptidase Inhibitor 1
TOC - Time of Contact
TOR - Time of Removal
UCSD - University of California, San Diego
UMAP - Uniform Manifold Approximation and Projection
VEGF - vascular endothelial growth factor
vSMCs - vascular Smooth Muscle Cells
wt - wildtype

1. Introduction

1.1. Fibrosis in Solid Organs

Response to tissue injury in the body is a very intricate process with the goal to restore tissue homeostasis. It requires very tight spatial and temporal control of various specialized cell types to remove the cellular debris and maintain tissue integrity. (Borthwick & Wynn, 2015; Clarke, Carruthers, Mustelin, & Murray, 2013) At the site of injury, the resident structural cells, as well as blood-derived immune and progenitor cells are responsible for the acute inflammation response and subsequent wound healing. However, persistent injury and inflammation can lead to dysregulation of the fibrotic response and hence the parenchymal tissue is replaced with a robust fibrotic scar. (Borthwick & Wynn, 2015) Fibroproliferative disorders are a major cause of mortality in the developed society with some assessments stating that up to 45% of all deaths can be contributed to chronic fibrosis. (Sziksz et al., 2015) Disorders such as pulmonary fibrosis, renal diseases, inflammatory bowel disease, and cardiovascular or liver fibrosis all have a common characteristic of organ dysfunction due to excessive fibrous protein deposition in the extracellular spaces of damaged tissue. Stimulating proliferation and matrix formation has also been implicated as a hallmark of tumor cells through a phenomenon known as desmoplasia. (Bachem et al., 2005)

The pro-fibrotic environment is stimulated by various cellular and molecular mediators and other factors derived from the ECM such as mechanical tension and oxidative stress. (Mu et al., 2010) A summary of the current knowledge on fibrosis in the periphery is described below including the sources and role of scar-producing cells, the composition of extracellular matrix (ECM) scaffolding and the distinct mediators that drive the response. Having clear insight into the complex processes involved during pathological fibrotic formation following tissue injury in the human body can provide a better understanding of the ways scar-forming fibrotic cells and their mediator respond to ischemic injury in the CNS.

1.1.1. Mediators of Fibrosis

Fibrosis is described as excessive and pathological deposition of extracellular matrix proteins which leads to scar formation. Pro-fibrogenic mediators in different tissues are derived from cells, molecules such as growth factors, cytokines and from direct influences found in the ECM environment. (Mu et al., 2010) The schematic depiction of the interplay between various

profibrotic mediators can be seen in figure 1. Myfibroblasts are the main cell type that is responsible for ECM protein synthesis, remodeling and 3D matrix organization in the injured tissue. They also contribute to stimulation of the pro-fibrotic environment by producing a plethora of pro-inflammatory mediators and angiogenic factors. The sources and role of activated myofibroblasts are discussed in the next

section below. The profibrotic factors are also secreted by other activated immune cells found in the injured tissue such as infiltrating and resident monocytes/macrophages, T-lymphocytes and mast cells. These stimulating molecular factors act to irreversibly increase transcriptional activation and density of various ECM proteins. (Mu et al., 2010; Tidball, 2005) However, the chronic inflammation response also leads to inhibition of fibrosis by releasing anti-fibrotic molecules at the same time. TFG-b has been remarked a master driver of fibrosis by activating the ERK/cJun/p38,

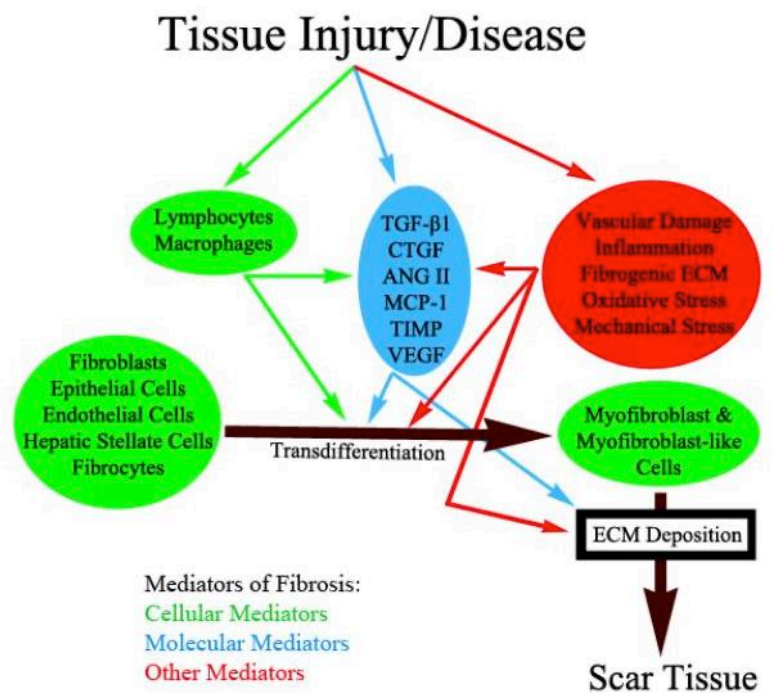


Figure 1. A diagram representative of the different factors that mediate fibrosis formation. Mediators of fibrosis: Cellular (green), Molecular (blue) and Other (Red). (Mu, Bellayr, Walters, & Li, 2010)

SMAD2/3 and other transcriptional pathways whose downstream mediators act profibrogenic. (Bonniaud et al., 2005; Mu et al., 2010) Other important released growth factors are platelet-derived growth factor (PDGF), connective tissue growth factor (CTGF), insulin-like growth factor (IGF), fibroblast growth factor (FGF), and epidermal growth factor (EGF) which all lead to increased myofibroblast differentiation and collagen protein deposition. Furthermore, other pro-fibrotic mediators are cytokines (IL-4, IL-5, IL-13, IL-21), chemokines (MCP-1, MIP-1 β), angiogenic factors (VEGF), acute phase proteins (SAP), caspases, components of the renin-angiotensin-aldosterone system (Angiotensin II/ANG II) and more. (Sziksz et al., 2015; Wynn, 2008) Metalloproteinases or MMPs which induce basement membrane breakdown and their inhibitors (TIMPS) can be used as indicators of fibrosis severity. (Mu et al., 2010) Altered profiles of fatty acid metabolism have also been implicated in pathophysiology of chronic fibrotic disease such as idiopathic pulmonary fibrosis and can be used as IPF biomarkers. (Suryadevara, Ramchandran, Kamp, & Natarajan, 2020)

The complex orchestrated interactions of the damaged microenvironment also contribute to the pro-fibrotic state. Tissue damage is almost synonymous with vascular injury which initiates the wound healing response by upregulating pro-inflammatory factors, blood clot formation and induction of transdifferentiation of myofibroblasts. (Kisseleva & Brenner, 2008) Subsequent inflammation recruits peripheral immune cells like macrophages and lymphocytes to the site of injury to remove cellular debris and further upregulate expression of cytokines, chemokines, angiogenic and other pro-inflammatory factors. (Tidball, 2005) Furthermore, NADPH upregulation at the site of trauma indicates oxidative stress which promotes fibrosis by promoting TGF- β upregulation and causing dysregulation of MMPs and its inhibitors. (Kinnula, Fattman, Tan, & Oury, 2005) Lastly, the 3D fibrotic scaffolding and the mechanical tension that is present supports and stimulates adhesion, migration, proliferation, transdifferentiation and inflammation. (Schuppan, Ruehl, Somasundaram, & Hahn, 2001)

1.1.2. Sources and Role of Myofibroblasts

Fibroblasts are found in connective tissues throughout the body and are imperative for tissue support and homeostasis. They express a variety of structural and adhesive proteins, as well as ground substances such as hyaluronan and glycoproteins. Fibroblasts are implicated to have critical function in ECM maintenance, wound healing, inflammation, angiogenesis, cancer progression, and in physiological and pathological tissue fibrosis. (Kendall & Feghali-Bostwick, 2014) Fibroblasts can be activated by paracrine and/or autocrine signals and pathogen-derived PAMPs which interact with toll-like receptors on fibroblasts. (Wynn, 2008) Moreover, they are involved in the wound healing response by initiating hyper ECM deposition and secretion of proinflammatory mediators. The transformation of fibroblasts to myofibroblasts leads to upregulated expression of scar-producing genes, expression of contractile machinery and hypersensitivity to growth factors and other mediators. (Kendall & Feghali-Bostwick, 2014) Cytokines that are produced by myofibroblasts include TGF β , VEGF, CTGF, IL-1, IL-6, and IL-8 which help fulfill its role in wound healing. (2018) Phenotypic expression of myofibroblast markers is used for cellular identification in IHC. Myofibroblasts express high amounts of α -smooth muscle actin (α -SMA), vimentin, smooth muscle myosin heavy chain and desmin. (G. Gabbiani, 2006)

Fibroblasts are not terminally differentiated mesenchymal derived cells. There are many sources of transdifferentiated myofibroblasts in the human body. Firstly, resident fibroblasts can be stimulated by TGF-b, IL-6, PDGF, Wnt, etc. to upregulate fibrotic gene expression. Moreover, myofibroblasts can arise from resident specialized mesenchymal cells such as endothelial cells, epithelial cells or pericytes through a process termed endothelial/epithelial to mesenchymal transition (EndMT/EMT). (van Caam et al., 2018) Finally, bone-marrow derived circulating progenitor cells called fibrocytes can also be stimulated by various cytokines, chemokines and GFs to migrate to the site of injury and induce transdifferentiation to myofibroblasts. Their phenotypic expression is characterized by CD34, CD45

and collagen type 1. (Wynn, 2008) Understanding which cell type(s) is the main contributor to the fibrotic response in various organs and the molecular mechanisms that drive them could provide novel therapeutic approach targets to treat individual fibrotic diseases.

1.1.3. Extracellular Matrix Scaffolding

The extracellular matrix is a very heterogeneous, non-cellular structure that maintains tissue elasticity, integrity and is crucial for homeostasis in normal physiology. It exhibits various functions including structural support, modulation of cell signaling and providing mechanical function to tissues such as cartilage, tendons and bones. (Arseni, Lombardi, & Orioli, 2018) In disease, myofibroblasts form very robust scaffold networks that can be stimulated and remodeled by activated cells and in turn stimulate them to respond by processes like migration. (Kendall & Feghali-Bostwick, 2014) Furthermore, matrix protein receptors such as integrins, syndecans, discoidin domain receptors and proteoglycans act to induce focal adhesion of myofibroblasts and immune cells, cadherin-mediated anchoring to the matrix and subsequent induction of ECM reorganization. Cellular adhesion is predominantly regulated by integrins which can sense the scaffolding, by interaction of specific ECM molecules, such as collagens and fibronectin. This in turn activates downstream intracellular signaling cascades including the focal adhesion kinase (FAK) signaling pathway, the mitogen-activated protein (MAP) kinases and the Rho family GTPases. (Arseni et al., 2018) The matrix associated receptors are essential for maintaining proper rates of stem cell differentiation and renewal. Moreover, the ECM has reservoirs of growth factors, angiogenic factors and cytokines to be able to deliver signaling mediators to recruited cells. (Arseni et al., 2018) The schematic depiction of the major ECM components and their interactions with each other are described and seen in figure 2 below.

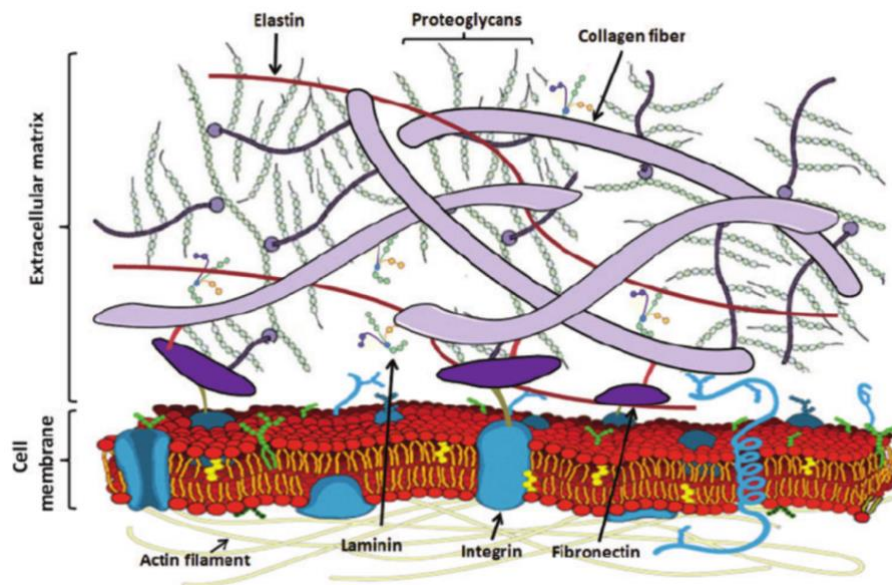


Figure 2. Major extracellular matrix components and their interactions with each other and cell membrane post cutaneous injury. The main ECM components depicted are collagens, proteoglycans, fibronectin, laminin and elastin, as well as the integrin ECM receptors. (Xue & Jackson, 2013)

The specific molecular composition of the ECM can slightly differentiate in separate organs during physiological and pathological events, but the core matrisome is known to be comprised of over 300 proteins. The main constituents of the 3D matrix are proteoglycans (also known as glycosaminoglycans, GAGs), adhesive glycoproteins and fibrous proteins. GAGs are part of the ground substance and contain a protein core with attached carbohydrates. (Arseni et al., 2018) They can interact with other ECM proteins or GAGs and thus induce transcription of mediators implicated in cell development and signaling, inflammation and wound healing. (Hynes & Naba, 2012) One of the most abundant proteoglycans found in human tissues is hyaluronan (HA) which also contributes to tissue hydration and lubrication. It acts as a prominent signaling molecule that mediates various biological processes such as adhesion, migration, differentiation and proliferation. (Hari Garg, 2004)

The association between cells and the ECM is primarily driven by adhesive glycoproteins such as fibronectin and laminin. Fibronectin is essential for collagen production, bridging together various ECM proteins and also contributes to the regulation of immune response by controlling amount of TGF- β present at the site of injury. (Arseni et al., 2018) Fibronectins bind to other core constituents such as collagens, heparin sulphate proteoglycans (HSPGs) and specific integrins found on the cellular membranes through interaction with the RGD motif domain. (Kendall & Feghali-Bostwick, 2014) Laminins are composed of α -, β - and γ - subunits and also contribute to cellular behavior such as direct migration. (Hamill, Kligys, Hopkinson, & Jones, 2009)

Fibrous proteins found in the ECM are various fibrillar and non-fibrillar collagens and elastin. Elastin is secreted as tropoelastin and is the key effector protein that provides tissue elasticity and flexibility. (Mithieux & Weiss, 2005) On the other hand, collagens are the major fibrous proteins that provide structural support, elasticity and strength in many tissues and interestingly, account for $\frac{1}{4}$ of total protein mass. There are 28 different collagens identified which are synthesized as procollagen precursors, formed from over forty genes encoding an alpha chain. (Arseni et al., 2018) N- and C- terminal peptides are cleaved from the procollagens which allow for the assembly of tropocollagens into collagen fibrils and subsequent large fibers. (Lodish et al., 2000) A characteristic of all collagens is the assembly of three distinct alpha chains. Moreover, collagens are classified as fibril-forming collagens (e.g., types I, II, III), network-forming collagens (e.g., type IV), fibril-associated collagens with interruptions in their triple helices, or FACITs (e.g., types IX, XII), and others. (Yue, 2014) The robust fibril scaffolding is resistant to degradation derived from pathogenic collagenases and peptidases; however, the 3D scaffolding undergoes consistent degradation, synthesis, assembly and remodeling during tissue homeostasis. (Arseni et al., 2018) Cleavage of collagens and other ECM biological constituents is mainly performed by matrix-metalloproteinases (MMPs), cysteine cathepsins and serine proteinases. Followed by

subsequent phagocytosis of apoptotic cells and cellular debris. (Everts, van der Zee, Creemers, & Beertsen, 1996)

1.2. Stroke – Types and Causes

Stroke is one of the leading causes of death and permanent disability worldwide. In the United States and Europe alone, more than 1.45 million people suffer from stroke each year. Stroke can be broadly classified into ischemic and hemorrhagic stroke. According to the CDC data, ischemic stroke accounts for 86% of all stroke cases and occurs when the brain is subjected to hypoxic conditions due to blockage of blood supply the brain parenchyma. (Musuka, Wilton, Traboulsi, & Hill, 2015) If the blood flow has been blocked for a very short period of time – under 5 minutes, then the event is called a transient ischemic attack or 'mini-stroke'. (Coutts, 2017) On the other hand, hemorrhagic stroke happens when an artery in the CNS leaks, ruptures or bursts allowing for the blood to saturate the parenchyma and cause damage. There are 2 main types of hemorrhagic stroke characterized as intracerebral hemorrhage and the less common type, subarachnoid hemorrhage. (Unnithan AKA, 2020) Stroke risk significantly increases with age; however, strokes can occur at any age. (Campbell et al., 2019) According to CDC statistics, increased incidence and mortality from stroke is seen in Black and Hispanic populations in the U.S. Additional major risk factors for stroke are sex, genetic predispositions, lifestyle choices such as smoking, and the experience of a previous ischemia or hemorrhage in the CNS. (Parmar, 2015)

Ischemic stroke is accompanied by a neurological deficit caused by acute focal injury to the CNS - spinal cord, brain and retina. The acquired disability or functional deficit is dependent on the region of brain affected by ischemia. The most common initial signs of stroke are confusion, loss of speech or aphasia, lateral hemiparesis, loss of coordination, balance and lateral motor control. Ischemic stroke is most commonly caused by thromboembolism derived from cardiovascular diseases such as

atherosclerosis and atrial fibrillation. Other sources that can cause CNS stroke are arteroembolic or large-artery disease, lacunar or small-vessel disease and others. (Musuka et al., 2015) Cerebral venous infarction is very rare; however, it is commonly a secondary event following cerebral venous thrombosis or following a hemorrhagic stroke. (Campbell et al., 2019) Brain imaging is the first and most important step in diagnosing and differentiating between the type and location of stroke which then should ultimately lead to the application of proper therapeutic approach.

1.2.1. Ischemic Stroke – Ischemic Cascade and Phases of Recovery

Upon ischemia in the CNS, there is extensive temporal and spatial organization in 2 distinct areas – the penumbra or the peri-infarct area characterized by slight hypoperfusion and the infarct core region where there is irreversible neuronal and glial damage. (Dirnagl et al., 1999) Collateral blood flow allows for the blood to reach the periinfarct areas after artery occlusion. There is variation in the extent of collaterals in individuals which causes discrepancies between stroke recovery outcome. (Campbell et al., 2019) The complex cascade of events which causes tissue injury following ischemia is shown in figure 3 below. Focal cerebral hypoperfusion initiates neuronal excitotoxicity which leads to oxidative stress, microvascular injury, inflammation and blood-brain-barrier (BBB) dysfunction. The degree and duration of the ischemic event determines the severity of the cerebral damage. (Lakhan, Kirchgessner, & Hofer, 2009) Reperfusion to the injured tissue is either caused by therapeutic or spontaneous clot breakdown. The reintroduction of blood into the site of injury also contributes to BBB breakdown and enhancement of immune cell infiltration from the peripheral circulation – known as the reperfusion injury. (Campbell et al., 2019)

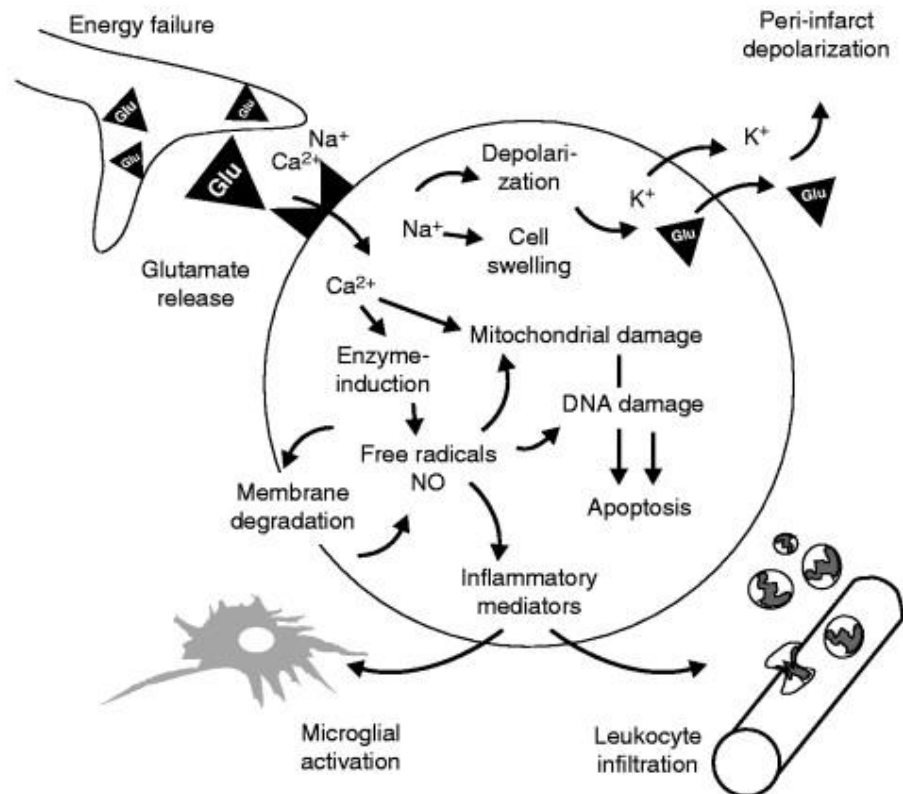


Figure 3. Simplified schematic overview of the pathophysiological mechanisms in the focally ischemic brain. (Dirnagl et al., 1999)

When the presynaptic neuron becomes ischemic, it depolarizes causing dysregulation of the sodium/potassium pump. Depolarization in turn causes the opening of voltage-gated calcium channels, and the subsequent increase of intracellular calcium in the presynaptic neuron. This provokes the release of glutamate from the presynaptic vesicles into the synaptic cleft. (Lakhan et al., 2009) Glutamate binds to various receptors on the postsynaptic neuron such as NMDA, AMPA and MGLUR receptors which further cause dramatic increase in intracellular Ca^{2+} , Na^+ , Cl^- ions. Potassium ions are released into the extracellular space and their diffusion propagates peri-infarct depolarizations. (Dirnagl et al., 1999) The ion disbalance in the postsynaptic neuron leads to overexpression of numerous enzymes such as proteases, endonucleases, lipases, etc. which directly contribute to cellular death and damage. Upon reperfusion, endothelial cells upregulate leukocyte adhesive molecules contributing to the invasion of circulating inflammatory cells to the site of injury. (Lakhan et al., 2009) The ischemic neurons, glial cells and inflammatory cells all produce free radicals

that impair cell membranes, DNA and mitochondria and trigger the release of enzymes and mediators. Furthermore, MMPs additionally degrade the basement membrane surrounding the vasculature which enhances inflammation and edema/swelling. (Dirnagl et al., 1999)

Recovery from stroke is separated into distinct phases: the hyperacute phase (0-24 hours post ischemia), acute (lasting up to 7 days post ischemia), subacute (up to 6 months of recovery) and finally the chronic phase. (Grefkes & Fink, 2020) How the cascade of events impacts the tissue over time is depicted in figure 4. In the hyperacute phase of stroke, excitotoxicity contributes to neuronal and glial damage. Additionally, there is a plethora of mediators are released which are partly responsible for the extensive tissue damage and the delayed response mechanisms of programmed cell death and inflammation. Patients can experience significant improvements in recovery after the brain has had a chance to heal for a couple of weeks with a plateau of recovery already commonly observed after 3 months of recovery. (Grefkes & Fink, 2020)

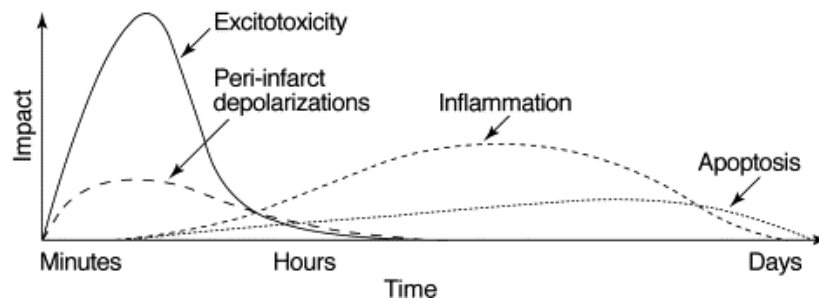


Figure 4. Timecourse of the damaging event cascades in focal cerebral ischemia. (Dirnagl et al., 1999) The x-axis shows the progression of the cascade over time, while the y-axis illustrates the impact of each element of the cascade on final outcome.

1.2.2. Therapeutic options for Ischemic Stroke

The main goal of therapy in acute ischemic stroke is to induce tissue preservation by reperfusion of blood into the peri-infarct regions. Up to date, only pharmaceutical and mechanical thrombolytic therapy is used as immediate treatment. To receive thrombolysis, the patient must meet specific criteria including a narrow time of onset window (up to 4.5 hours) and exclusion of intracranial hemorrhage by brain imaging. (Hurford, Sekhar, Hughes, & Muir, 2020) Recombinant tissue-type plasminogen activator or rt-PA has initially been FDA approved in 1996 and no new novel therapeutic options have been provided since then. Rt-PA is administered intravenously and acts to clear the occluding clot or embolism and restore blood supply to injured area. Furthermore, surgical endovascular intervention is also used to mechanically remove the clot and recanalize the artery or vein. (Bhatia et al., 2010) Following thrombolytic treatment, patients are often advised to take a polypill which includes statins to reduce LDL cholesterol, antiplatelet drugs to prevent subsequent clotting during recovery and also depending on patient prognosis, drugs to reduce blood pressure. (Brainin et al., 2018)

Current therapies are based on acute thrombolytic treatment and management of acquired deficits. However, every month, dozens of studies are published which show smaller infarct sizes and improved motor recovery by targeting cytoprotective mechanisms to preserve the brain tissue. However, extensive translational failure to clinical research for thousands of molecules has provided a lot of cynicism to field experts. A lot of challenges in stroke preclinical and clinical research have led to the establishment of STAIR (Stroke Therapy Academic Industry Roundtable), which aims to provide recommendations which outline priorities for future stroke studies. (Jovin Tudor, Albers Gregory, Liebeskind David, & null, 2016) A common underlining issue is consistency during basic research and clinical trials. Firstly, clinical trials are based on including subjects from a specific population with a very short time of onset window and with specific vessel occlusion. (Zerna, Hill Michael, & Boltze, 2017) The same criteria should

also be present in preclinical studies. Furthermore, the exact mechanism of neurorecovery must be elucidated to possibly target specific components which respond in positive recovery outcome post-ischemia in the CNS. (Zerna et al., 2017) Substantial differences in stroke recovery have been described for females and males, also dependent on the age of onset. Most studies are performed in male mice and hence, neuroprotective mechanisms should be elucidated for both sexes in different age groups following ischemic stroke. (Brait et al., 2010) A study from 2019, even showed that circadian rhythm of model organisms affects the mechanisms of disease and response to therapeutics. (Esposito et al., 2020) Most studies are performed during the day when the most common model organism, the mouse, is in its inactive phase. Contrastingly, humans experience stroke more often during their active cycle which also contributes to lack of translation. Many more variations are known to affect both preclinical and clinical research, therefore, future research should aim to maintain as consistent dataset as possible across all phases of research and also to provide more comprehensive understanding of all various pathological mechanisms during stroke recovery.

1.3. Fibrosis in the CNS

Fibrosis is a part of a critical response to injury in the CNS and has been described in spinal cord injury, EAE (multiple sclerosis model), stroke and traumatic brain injury or TBI thus far. The exact cell type that forms this scar has been debated, with various sources claiming it arises from a variety of perivascular cells. Pericytes have been widely observed to play important roles in the development and maintenance of the blood-brain barrier, regulation of transcytosis, aiding in tissue clearance and more. (Daneman, Zhou, Kebede, & Barres, 2010) Furthermore, a subtype of pericyte using a Glast-CreER reporter mouse (noted as 'type A'), has been shown to upregulate collagen expression in disease and form the fibrotic scar following spinal cord injury. (Göritz et al., 2011a) However GLAST is

also expressed in fibroblasts and thus they may have misidentified them. Conflicting studies showed that pericytes do not substantially proliferate following CNS injury and are not the major contributors of ECM in fibrotic scar after ischemia. (Cano, Gebala, & Gerhardt, 2017; Roth et al., 2020) Recent data from (Dorrier et al., 2021) has shown that fibroblasts similar to parenchymal fibroblasts are present in the meninges and perivascular spaces of the brain and spinal cord and are the primary source of the CNS fibrotic scar.

CNS fibroblasts are located in the in the dura, arachnoid and pia mater of the meninges as well as in the Virchow-Robin space. (Lam et al., 2017) Most studies use GFP in the Col1a1GFP reporter mouse to label CNS fibroblasts. Marker specificity remains a problem in the field and finding a specific marker for fibroblasts throughout the body has been difficult. PDGFRB is often used as a marker for pericytes, but because it is also present in fibroblasts it may be contributing to the functions described of PDGFRB+ cells. (Dorrier et al., 2021) The ER-TR7 antigen on reticular fibroblasts and their adjoining extracellular network is often used to mark fibroblasts, although the molecular identity of this antigen is unknown. (Van Vliet, Melis, Foidart, & Van Ewijk, 1986) Our research has observed a very high degree of overlap in Col1 and ER-TR7 staining, therefore more specific markers could substantially help in identification and differentiation of cellular populations. Fibroblasts in the CNS are much more abundant in the meninges than in perivascular spaces and have been shown to play structural support roles within and between the different meningeal layers. (Kendall & Feghali-Bostwick, 2014) The role of perivascular fibroblasts in the Virchow-Robin space and surrounding blood vessels in the subarachnoid space is less understood. A paper from Vanlandewijck et al., was the first to characterize these cells was a comprehensive single-cell sequencing study of the brain vascular and perivascular cells in healthy mice (Vanlandewijck, 2018). They found 2 clusters of fibroblasts which they denoted as 'fibroblast 1' and 'fibroblast 2'. These fibroblasts highly express extracellular matrix proteins such as collagens but show preferential expression for Col15a1

(fb1) and Itga8 (fb2). Further studies are needed to characterize the role of these cells in the healthy CNS and following injury.

Other perivascular cell types have been implicated in wound repair in the CNS. During numerous forms of CNS trauma, astrocytes undergo reactive astrogliosis which is considered as a hallmark pathological response and characterized by gene expression changes, hypertrophy of cellular body and protrusions, proliferation, scar formation and long-term organizational changes. (Li et al., 2020) Moreover, perivascular macrophages (PVMs) react in various neurological disorders and injuries and have been implicated to contribute to fibrosis. PVMs have shown to alter their phenotype upon tissue injury to induce the transcription of pro-inflammatory mediators (TNF- α , IL-6 and IL-1 β) which can activate fibroblasts and induce growth, migration and subsequent secretion of ECM proteins. (Mescher, 2017) Lastly, smooth muscle cells have been implicated in fibrosis in various pathologies throughout the body with the most common including atherosclerosis and asthma. (Hu, Yin, Luo, Habenicht, & Mohanta, 2019) However, studies have shown that vSMCs do not contribute to fibrosis following neuroinflammation. (Dorrier et al., 2021)

1.3.1. Astroglial and Fibrotic Scarring in Ischemic Stroke

Following triggers in the CNS such as inflammation, injury or hypoxia, a scar forms around the site of trauma consisting of 2 parts: a glial scar made up of reactive astrocytes that form almost immediately after injury and an inner fibrotic scar in the disease core that seals up the injury site and forms in the days and weeks following the trigger. (Fernández-Klett & Priller, 2014) This glial scar has been widely characterized, and new research shows that it has an overall beneficial role in disease repair. The inner fibrotic scar has been much less studied although has also been implicated in disease repair and recovery following injury and inflammation in the CNS. Recently, strong evidence shows that the origin of this fibrotic scar is CNS fibroblasts. It has been shown that both PDGFRB⁺ and

Col1a1GFP cells, increase in number in the lesion core surrounded by fibrotic proteins following the MCAO mouse model of stroke. (Fernández-Klett & Priller, 2014; Kelly et al., 2016) These cells have now been identified as fibroblasts but the origin of fibroblast like transcriptional profile has yet to be fully determined. The glial scar surrounding the infarct core is described and seen in figure 5 below.

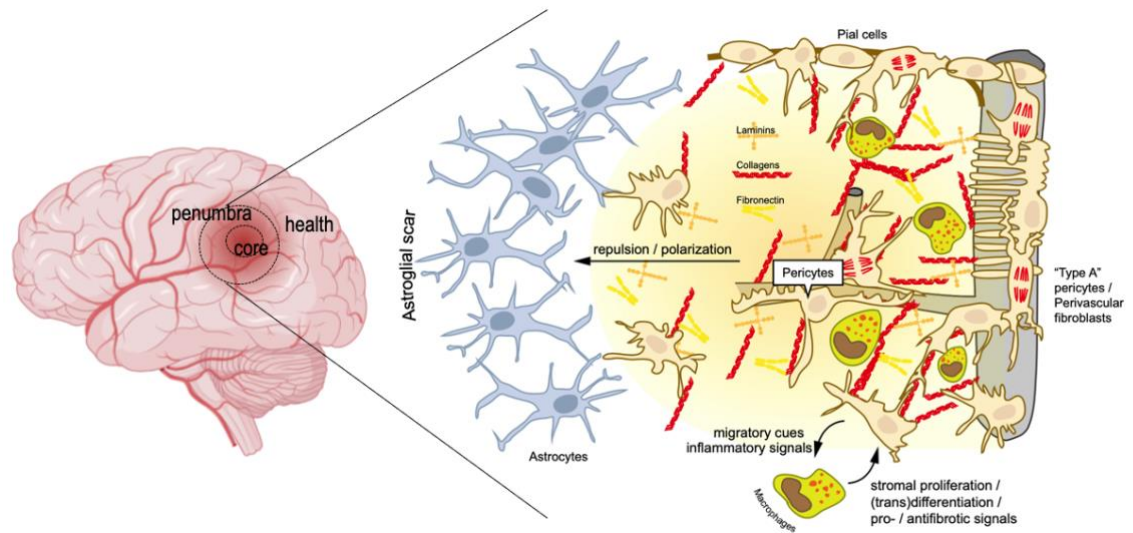


Figure 5. Schematic depiction of the astroglial scar surrounding the infarct core following ischemic stroke and the subsequent cellular and molecular interactions in scar formation. Created with BioRender.com and (Fernández-Klett & Priller, 2014)

When the blood supply is blocked to a certain part of the brain, astrocytes respond immediately by undergoing morphological modifications such as hyperplasia and hypertrophy and also show high rates of proliferation and increased expression of the intermediate filament proteins including GFAP, vimentin and nestin. (Z. Liu & Chopp, 2016) The glial scar forms a physical and functional barrier between the necrotic brain tissue and the rest of the parenchyma. This acts to control the inflammation response and restrict cells and its mediators to the site of injury. (Z. Liu & Chopp, 2016) The astroglial scar is separated from the fibrotic scar found in the ischemic core. The fibrotic scar has been shown to display high rates of ECM protein deposition which are usually expressed in low amounts

throughout the healthy parenchyma. In the lesion core, inflammatory and fibroblast cells interact to form a robust fibrotic scar. The scar is mostly composed of collagens and glycoproteins such as fibronectin and laminins, which is consistent with ECM scaffolds found in pathological peripheral organ fibrosis. (Fernández-Klett & Priller, 2014) Studies have suggested that the ECM acts as mechanical support to the tissue, but has a detrimental role by limiting anatomical plasticity of neural networks. (Fernández-Klett & Priller, 2014) Our research hopes to provide answers for the specific role and function of the fibrotic scar.

1.4. Aims and Problem Statement

Recently, a small number of studies have reported that following stroke, a fibrotic scar forms in the infarct area that is similar to the scar identified in CNS spinal cord injury. Little is known about the role of the fibrotic scar in repair following stroke and the signals that activate scar formation. Our goal is to define the role of the fibrotic scar in repair following stroke and the molecular mechanisms that are responsible for its formation. This could potentially lead to identifying potential therapeutics to manipulate the scar in humans. The Daneman lab has already performed lineage tracing experiments in the EAE mouse model and found that the fibrotic scar lasts for months after the autoimmune lesion formation and is formed from the expansion of CNS fibroblasts. (Dorrier et al., 2021) The goal of this research is to determine the mechanisms that drive fibrosis in stroke.

This scar tissue could have an impact on how the brain can recover following stroke by blocking therapeutic agents from reaching the injured site in the brain or limiting axonal sprouting. We hypothesize that preventing the fibrotic scar from forming will increase repair following stroke. It has been speculated that the fibrotic scar acts in detriment to the CNS due to the high ECM matrix content potentially limiting brain plasticity needed for learning and memory throughout life. The outcomes of this

project have the potential to lead to new therapeutics that could aid in recovery following stroke. If we find that manipulating a signaling pathway has the ability to reduce fibrotic scar formation following a stroke in mice, leads to a more thorough recovery following the stroke, than the pathway could be targeted in a clinical setting for human patients who have recently had a stroke to aid in their recovery. Alternatively, if we find that inhibition of fibrotic scarring leads to decreased recovery, then we can develop methods to enhance fibrotic-scar derived recovery by targeting specific pathways.

We wanted to answer several questions previously undescribed in stroke concerning fibrotic scarring found in the ischemic core. Firstly, we wanted to determine when fibrotic scarring starts to form in response to ischemia in the CNS, if there is stabilization or clearance of ECM and how long does it persist after the event. Secondly, we wanted to determine the main cell type responsible for ECM deposition. Single-cell RNA sequencing has been performed to gain insight into the transcriptional profile of the collagen-producing cells and the molecular mechanisms that drive fibrosis in the CNS. Subsequently, we wanted to see how the fibrotic response differs from the response in the peripheral solid organs. Furthermore, to assess the implication of the scar tissue in recovery we have ablated scar producing cells post dMCAO and evaluated sensorimotor recovery post cortical ischemia. The insight will be gained whether the scar acts in a neuroprotective or neurotoxic phenotype.

2. Materials and Methods

2.1. Experimental model and Subject details

Inbred strain C57bl/6 (B6) from Jackson Labs 029567 was used for evaluating the fibrotic and inflammatory response of the infarct core tissue post dMCAO in a time course of 30 days. Col1a1GFP mice from David Brenner (C57bl6 background) were utilized to label Col1 producing cells for FACS sorting and scRNA sequencing analysis. B6;129S7-Hprt1^{tm2(Pgk1-Pac/Tk)}Brd/Mmucd, MMRRC 010860-UCD (C57BL/6Try c-Brd mixed background), (lox-stop-lox-HTK) mice were crossed to Col1a2CreERT, Jackson Labs 029567 (C57BL/6 background) for experiments aiming to ablate dividing fibrotic cells. All animal protocols were approved by IACUC at UCSD and all ethical regulations have been followed in the use of mice for this study. Male mice were used for all experiments to limit stroke outcome variability.

For the time-course experiments, focal ischemia was induced in the right hemisphere in adult mice between 12-15 weeks of age. Mice for all other experiments were between 3 and 9 months of age at the start of dMCAO. For ablating the proliferating fibroblasts, all test and control mice received intraperitoneal (IP) injections of 2 mg tamoxifen in sterile corn oil for 3 consecutive days at 6 weeks of age to induce CreERT mediated excision of the lox-stop-lox cassette. CreERT is expressed by Col1a2 expressing cells and is sensitive to tamoxifen administration. Furthermore, ganciclovir (Acros Organics, AC461710010; Milipore Sigma, Y0001129) was administered daily between 8-10am for 30 consecutive days through subcutaneous injections in the inguinal region of a scruffed animal. All males were used as the HTK gene is X-linked, n = 13 control (HTK) and 7 test (HTK+Col1a2-CreERT). Two test mice were euthanized due to extensive subdural hemorrhaging during microsurgery, so the data was not included. The first ganciclovir injection day occurred 24 hours prior to the microsurgery - distal middle cerebral artery occlusion (dMCAO) accompanied with 60-minute CCA clamping. All mice were housed at the Leichtag Biomedical Research facility at UCSD in a temperature-controlled

environment at 20 to 22 degrees Celsius, 40-70% humidity and a 12-hour light/dark cycle.

2.2. Distal Middle Cerebral Artery Occlusion + 60min microvascular clamping

To provoke a brain injury that simulates a focal ischemic event comparable to the severity of stroke that occurs in many humans, the distal branch of the middle cerebral artery was cauterized. To stimulate an ischemia-reperfusion insult, blood flow was restricted for 60 minutes by using a metal vascular clamp on the right CCA. The release of the clamp 60 minutes post dMCA coagulation also allows for less bleeding during surgery and subsequently less tissue damage.

Firstly, a dose of Buprenorphine SR/Lab (1mg/kg 1uL/g mouse, typically 20-30uL; ZooPharm BZ8069317) was given subcutaneously at the interscapular region of the mouse 30 minutes prior to anesthesia administration. The surgical area was setup, and the mice were placed in the anesthesia box saturated with 2% isoflurane at flow rate of 2L/min medical O₂. The surgical area between the right eye and ear of the mouse was shaved and sterilized with Betadine Surgical Scrub (Providone-iodine, 7.5%) and 70% alcohol swabs. Furthermore, eye ointment was applied, and the mouse was monitored for the pedal reflex, eye/blink reflex and respiratory rate. An incision was made between the eye and ear and the ligaments attached to the temporal muscle were severed using vannas scissors. The temporal muscle was subsequently scrapped until the zygomatic root became visible. Next, a craniotomy was performed using a micro drill exposing the distal branch of the MCA. Once the vessel was exposed, the mouse was turned onto its back and the surgical site of the neck was sterilized. The skin was separated, and the left and right submaxillary glands were detached to visualize the trachea, common carotid artery and internal jugular vein. The CCA was isolated from the attached vagus nerve and fat tissue, and the metal micro clamp was secured on the

CCA (Figure 6.d). The mouse was quickly returned to its site and the MCA vessel was coagulated using a bipolar coagulator at the proximal location directly before the branching point of the distal MCA at the site of craniotomy (Figure 6.c). The surgical site was closed using VetBond Tissue Adhesive (006245) and the mouse was placed into the anesthetic chamber for 60 minutes. Next, the clamp was released, and the surgical side closed with Vetbond. Finally, the mouse was transferred to the post-operative box placed on a warm heating pad (37°C) until ambulatory. Sham littermate controls have been subjected to surgery conditions, but dMCA cauterization and CCA clamping was not carried out. Mice were monitored for activity, pain and signs of inflammation for 5 days post-op. Lidocaine ointment USP, 5% (NDC 50383-933-35) was applied at incision site when necessary.

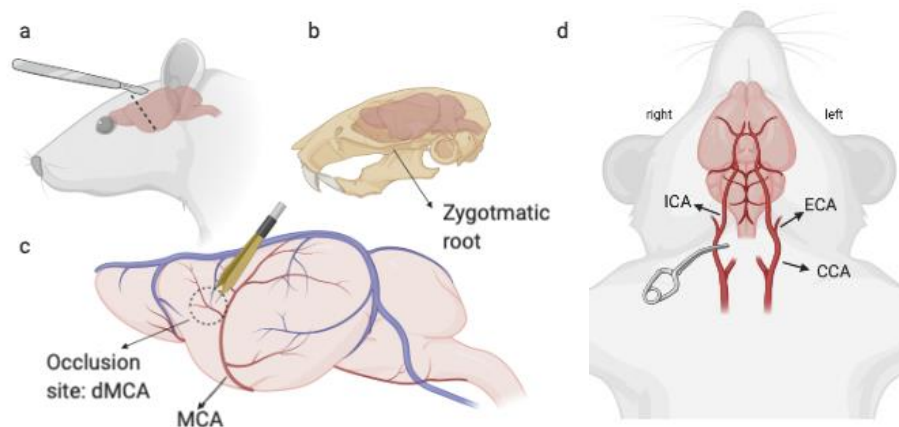


Figure 6. Schematic depiction of distal middle cerebral artery perfusion in combination with 60-minute clamping time where the a) surgical incision site is shown with the b) zygomatic root being the orientation guide in dMCAO microsurgery. c) The occlusion site is depicted, and in the dotted area, the proximal position below the vessel branching is the site of cauterization. To cause a reperfusion insult, a metal clamp was placed securely in around the right isolated CCA as shown in d). *Created with BioRender.com*

2.3. Tissue Processing

2.3.1. Whole Animal Perfusion Fixation and Drop Fixation

Rodents prepared for whole animal perfusion were anesthetized with an intraperitoneal injection of a Ketamine/Xylazine cocktail (~100 mg/kg Ketamine ("Zetamin" MWI/VetOne 501072), at 4 mg/mL; ~15 mg/kg Xylazine (AnaSed®), at 0.6 mg/mL). When the animal hasn't responded with a reflex response to a toe-pinch test, the procedure was started. The mouse was laid flat onto its back and the thoracic cavity was exposed by dissecting the diaphragm and rib cage. A 21G needle was inserted and stabilized into the left ventricle of the heart followed by an incision made onto the right atrium. The transcordial perfusion was setup as a 2-minute 1xD-PBS (Dulbecco's PBS) rinse followed by 9 minutes of pumping 4% Paraformaldehyde (PFA) with a peristaltic pump (Rainin Dynamax RD-RP1) set at 36 rpm to match the cardiac output of the mice. Successful perfusion was characterized by the clearing of the blood saturated liver, clear/white lung color and a rigid tail/body. The brain of the animal was carefully dissected from the calvarium and placed into a 5mL sample tube filled with 4% PFA for O/N at 4 degrees Celsius. Drop-fixation was implemented since the vasculature in the infarct region is impaired and 4% PFA couldn't saturate the tissue of interest adequately through perfusion-fixation.

After an overnight fixation step, the brain was washed 3 times for 5 minutes in 1xPBS and placed into 30% sucrose for 48 hours to limit tissue damage caused by ice crystal formation in the process of freezing. After the brain has been thoroughly saturated with the sugar solution, it is embedded into an OCT:30% sucrose solution = 2:1, frozen with dry ice and subsequently stored at -20 degrees Celsius.

2.3.2. Tissue slice collection

The frozen embedded sections were cut in a cryostat (Leica CM1950) at -23 degrees Celsius. The sections were refined into a cube and sliced in the coronal plane. Tissue collection was started between anatomical point-bregma 1.18mm to 1.8mm and finished between bregma -1.74mm to -1.92mm depending on the visual observation of the position of infarct on the rostral-caudal axis. 30-micron sections were sliced and transferred directly to a 24-well plate filled with a stock solution of 1XPBS with 0.02% Sodium azide to limit microbial growth. Floating sections were gathered until the infarct was no longer visually observable. Plates were sealed with parafilm and stored at -4°C for further analysis.

2.3.3. IHC staining

To evaluate the infarct size of the ischemic event provoked by dMCAO, the floating sections were stained with 1% Cresyl Violet Acetate solution which binds to Nissl substances in neurons. The floating sections were transferred from the 24-well plate to a 1xPBS waterbath and mounted onto a positively charged microscope slide. Each subsequent coronal section was 710 microns apart from each other, spanning affected and unaffected cortical regions. Once the sections have adhered to the slide and dried, the slide was rinsed in MiliQ water. The nissl staining procedure is carried out inconsequential steps of dehydration, rehydration, staining of tissue, destaining and finally, dehydration and clearing. All of the steps are performed under a fume hood as 5 minutes incubations of various ethanol solution concentrations (50-100%), cresyl violet solution, differentiation solution and xylenes. The slides are coverslipped with permanent DPX mounting medium, dried and stored at RT. The following day the microscopic images of the coronal sections are taken at 20x magnification with ZEISS Axio Zoom V.16 Microscope. Stitching was performed with Adobe Photoshop and resulting images are quantified with ImageJ/Fiji 1.52q software. The infarct volume calculation was performed via an algorithm by

McBride et al. which apart from taking into consideration the edema found in the infarct core region, also takes into account the peri-infarct area swelling. The algorithm can be seen below:

$$\text{Infarct Volume(\%)} = \left(\frac{\sum i \left(\left(\frac{I_i - N_i}{I_i} \right) C_i \right)}{2 \sum i C_i} \right) 100. \quad (1)$$

The areas of the contralesional (C_i), ipsilesional (I_i) and nonischemic ipsilesional hemispheres (N_i) were traced and the infarct volume from the algorithm was computed. All statistical evaluation was performed with Graphpad Prism Version 9.0.0. Ordinary one-way ANOVA with Dunnetts multiple comparison test was used to evaluate the infarct volume, while the hemisphere asymmetry and infarct core size was performed with one-way ANOVA and Tukey's multiple comparison test.

To perform immunohistochemical evaluation of formalin-fixed 30-micron thick floating coronal mouse brain sections, the sections were initially washed 3 x 5 minutes in 1xPBS/ 0.03% Triton/ 1% NGS solution (pH 7.4). Firstly, antigen retrieval with a heated buffer was performed to unmask epitopes for IHC staining. Sections were placed in an oven at 60°C in a pre-heated sodium citrate buffer (10mM Sodium citrate buffer, pH 8.5) for 30 minutes. For all plate transfers, we used Netwell™ inserts with 440 µm membrane mesh for 6-Well Cell Culture plates.

Heat-induced antigen retrieval was performed due to the additional drop-fixation step causing reduced detectability of proteins of interest for immunofluorescent analysis. Subsequently, the sections were blocked in 10% non-specific goat serum and permeabilized with 0.3% Triton in 1xPBS for 1 to 1.5 hours at RT in the dark. Followed by incubation O/N at 4°C on an orbital shaker (10 rpm) in primary antibody solution, composed of antibody buffer (NaCl 150 mM, Tris Base 50 mM, 1% BSA, L-Lysine 100 mM, 0.02% Sodium azide in water) and primary antibodies. The following

primary antibodies were used for all of the acquired evaluations: Collagen 3 (abcam, ab7778), GFAP (Invitrogen, PAI1-10004), ERTR7 (Novus Biotech, NB100-64932), CD31 (BD Bioscience, 553370), CD45 (Bio-Rad, MCA1031GA) and Iba-1 (Fujifilm Wako Chemicals, 019-19741). The following day the sections were washed and incubated with the corresponding secondary antibody in a 1:1000 dilution: Goat-anti-Rabbit-Alexa 488 (ThermoFisher A11034), Goat-anti-Rat-Alexa 488 (ThermoFisher A11006), Goat-anti-Rabbit-Alexa 594 (ThermoFisher R37117), Goat-anti-Rat-Alexa 594 (ThermoFisher A11007), in 1x PBS and incubated in dark at RT for 2-3 hours. Next, the sections were washed and mounted onto a positively charged microscope slide. After the slides have adequately dried, sections were rinsed with water to remove any residual salt found on the slides. DAPI Fluoromount-G (SouthernBiotech, 0100-20) was added and the slides were coverslipped and secured with nail polish. Images were taken with an Axio Imager D2 (Carl Zeiss) and digital camera (Axiocam HRm, Carl Zeiss) using the AxioVision software (AxioVis40 V 4.8.2.0), contrasted using Adobe Photoshop and quantified using ImageJ 1.52q Fiji. Processed and imaged slides are stored at -20 C.

2.4. Adhesive Tape Test

Preliminary analysis was performed where 3 behavioral tests were evaluated for sensitivity to dMCAO motor coordination deficits in mice post focal CNS ischemia. The rotarod test (Shiotsuki et al., 2010) and the capellini handling test (Tennant et al., 2010) were shown to be ineffective in statistically providing quantitative proof for motor impairment. However, the adhesive tape test (Bouet et al., 2009) was determined promising due to its high sensitivity at distinguishing the right and left paw coordination. This test measures the ability of mice to remove a small piece of tape from their paws and assesses fine motor function. The adhesive tape test trial was initiated by acclimating and habituating the test batches for 3 consecutive days prior to dMCAO and following the surgery the baseline is evaluated.

The procedure was started with acclimating the mice by individual placement into the test area - clear plastic box with a mirror on the bottom for 60 seconds. Adhesive tape was cut in 3 x 0.4 cm cube strips and placed onto the thenar, hypothenar, and interdigital pads of the scruffed animal. The trial was initiated once the animal was placed back into the test box area. In this experiment the following parameters were evaluated: overall duration time (maximum duration of 120 seconds is given to the animal to remove both adhesive strips), contralateral and ipsilateral contact time, and removal time. The contact time is defined as the point that the mouse reacts to the presence of the adhesive tape strips. Removal time is defined by the time the trial is started to the time the animal completely removes the strip from the respective pad. Three trials were conducted per animal for each trial day. An exclusion criterion was the presence of asymmetry of right vs left paw usage before the surgery of the overall cohort group. If the mouse did not remove one or both tape strips before the end of the trial, the trial was excluded from the quantification. Furthermore, very dramatic outlier trials were also excluded from the analysis. Two-way ANOVA with Tukey's correction for multiple comparisons in Graphpad Prism version 9.0.0 has been used to statistically evaluate the contralateral and ipsilateral paw contact and removal time post dMCAO. The significance of the ratios was also completed with a 2-way ANOVA with the Šidàk correction for multiple comparisons.

Twenty mice from each of the cohorts were given permanent distal MCAO surgery with 60-minute clamping time. The mice were monitored 5 consecutive post-OP days for vitals, activity level, signs of pain and evaluation on incision recovery. Mice that display good recovery were further monitored on behavioral testing days (day 3, 7, 14, 21 and 30 post-OP) until tissue collection which is 30 days post-dMCAO microsurgery. All strains are delivered with gancyclovir daily 25mg/kg daily subcutaneous for the length of the experiment. B6;129S7-Hprt1tm2(Pgk1-Pac/Tk)Brd/Mmucd, MMRRC 010860-UCD (C57BL/6Try c-Brd mixed background), (lox-stop-lox-HTK) mice were crossed to Col1a2CreERT, Jackson Labs 029567 (C57BL/6 background) for these experiment which

generated 9 test Col1a2CreERT2;lox-stop-lox-HTK mice and 10 control lox-stop-lox-HTK mice. The experimenter was blinded to the groups of the mice during the administration of ganciclovir, adhesive tape test and the following evaluation and analysis. In the results and discussion section below the two respective cohorts will be termed test (or HTK+Cre) and control (or HTK).

2.5. scRNA sequencing experiment

2.5.1. Tissue Dissociation and FACS sorting

To obtain scRNAseq data of scar-forming cells in health and MCAO, we first generated single cellular suspensions of the infarct and corresponding area for healthy mice. The brain was dissected from Col1a1GFP c57bl/6 mice on day 7 and day 14 post dMCAO + 60 min clamp. The healthy samples were derived from mice with same genotype, but no ischemia was induced. The infarct region was identified, extracted and chopped with a #10 blade. The broken-down tissue was enzymatically digested with papain (Worthington Biochemical, LK003176, 1 vial per sample) containing DNase (125 U/ml, Worthington LS002007) for 1.5 hours at 35°C. This was followed by mechanical trituration in a solution containing ovomucoid (2 mg/ml, Roche 109878) and DNase (125 U/ml) and second enzymatic digestion with 1.0 mg/ml Collagenase Type 2 (Worthington Biochemical, LS004176) and 0.4 mg/ml Neutral Protease (Worthington Biochemical, LS02104) at 35°C for 30 minutes. Subsequently, myelin was excised with myelin removal beads (MACS Miltenyi Biotec 130-096-433) and LS columns (MACS Miltenyi Biotec 130-042-401) on a MidiMACS separator (MACS Miltenyi Biotec 130-042-302). Suspensions were washed twice with buffer and live, Col1a1GFP+ cells were FACS sorted into Trizol (Invitrogen 15596026) based on GFP fluorescence using an ARIA II sorter at the Flow Cytometry Core at the VA Hospital in La Jolla, CA. Forward scatter and side scatter analysis were also used as gates to limit the sorting to single, live cells using FACSDiva v8 software.

2.5.2. Single Cell RNA sequencing and Data Processing

Collected samples include 2 healthy Col1a1GFP control male mice, 2 Col1a1GFP males that were collected 7 days post dMCAO and 1 Col1a1GFP male that was collected 14 days post-lesion induction. The dissociated and FACS sorted cells were collected into a PBS + 0.05% BSA solution and brought to the UCSD IGM core where the samples were run through the 10X Genomics pipeline (Chromium Next GEM v3.1) and sequenced on a NovaSeq 6000. The 10x Genomics pipeline includes consequential steps of generating and barcoding GEMs (Gel beads in Emulsion) through microfluidic forces, subsequent cleanup of leftover reagents and primers, cDNA amplification, 3' gene expression and library construction. The sequenced data was run through Cell Ranger 3.0.2 to generate counts data and Seurat v3 for filtering and clustering analysis. The resolution parameter of clustering was set to 0.5, and cells without any measurable Col1a1 or Col1a2 expression were filtered out of the dataset. $\log_{fc} \text{threshold} = 0.25$. SingleR was used to annotate single cells using the Immgen reference dataset. 4 clusters with low collagen expression and a transcriptomic profile of endothelial cells and microglia were also removed for further analysis.

3. Results

3.1. Timecourse of Fibrosis and Neuroinflammation in Stroke

3.1.1. Characterization of the Infarcts

To determine the size of the infarct in the dMCAO model of stroke over time in wild type C57bl/6 mice, we have performed Nissl staining on floating coronal sections to visualize neuronal survival. We evaluated infarcts of 16 test and 5 sham-operated mice by staining Nissl bodies with 1% Cresyl Violet (CV) solution. This technique was utilized to identify the affected ischemic regions in the mouse dMCAO model and to determine the percentage of the overall brain volume affected by the loss of neuronal structure and function. CV stains live and healthy neurons bright purple/blue color. However, the specificity of CV staining in the CNS is broadened to also stain chromatin and nucleolus structures of neuroglia and infiltrating cells with a darker violet color. (García-Cabezas, John, Barbas, & Zikopoulos, 2016) Representative images of the coronal sections for each post lesion day (PLD) can be seen in figure 7. Furthermore, we wanted to assess whether the performed dMCAO induced ischemia that replicates the patterns of atrophy and swelling in the brain according to other scientific literature. The swelling can occur in the non-infarcted ipsilateral hemisphere as well as the corresponding ipsilesional infarct region. Therefore, we evaluated the hemisphere volume asymmetry as seen in figure 7c below. The increase in lateral ventricular size after ischemia has been accounted for in the calculation (Sayed et al., 2020).

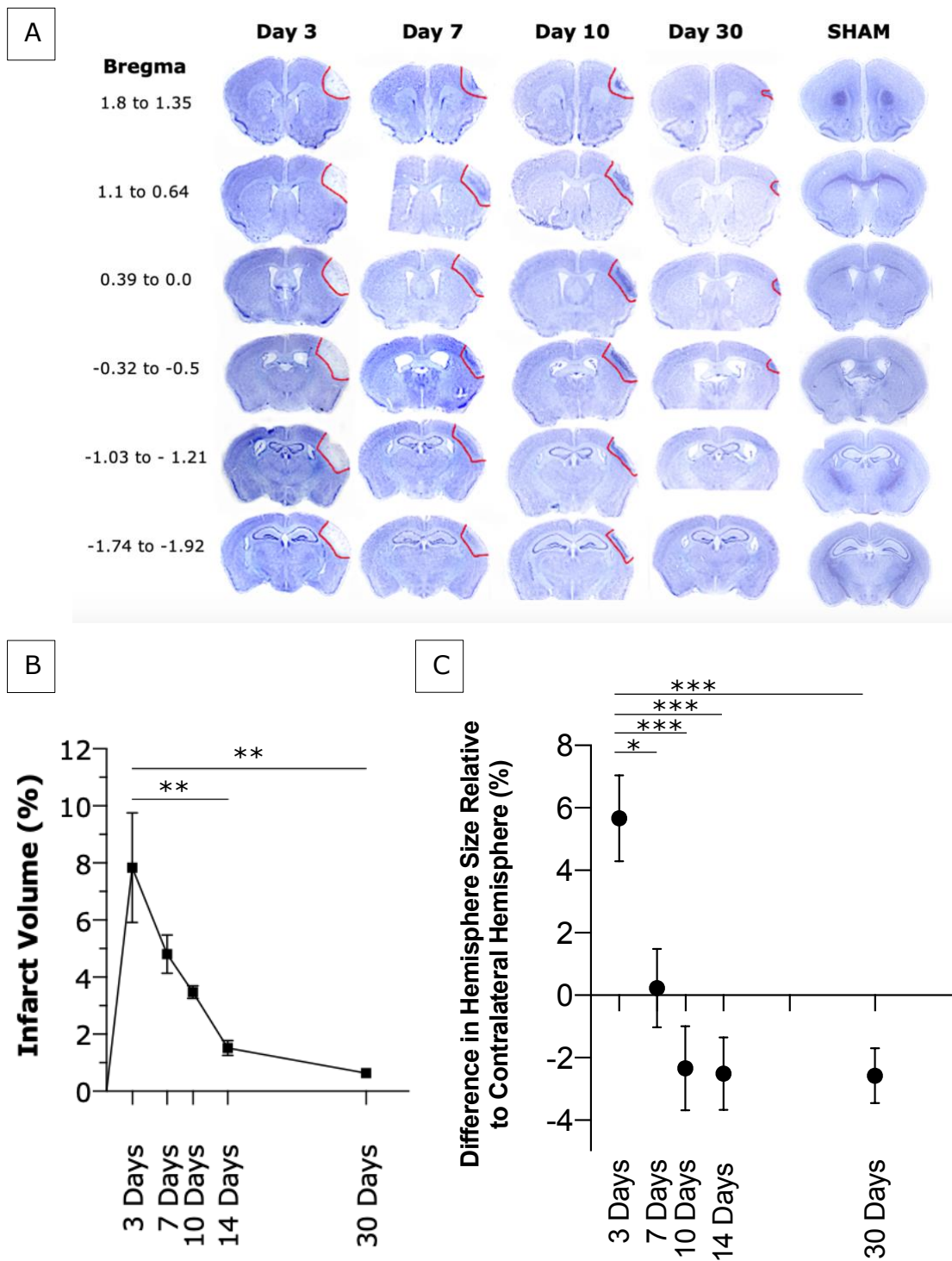


Figure 7. Characterization of infarcts by evaluation of cortical regionality, total brain volume affected and hemisphere asymmetry. (A) Colorimetric images of coronal brain sections stained with CV at different time points post-MCAO. Each column represents individual timepoints with the last column displaying the sham-operated mouse. Each

coronal section is 710 microns distanced from the following section. Line in red delineates the border between the presence and absence of CV signal indicating the area affected by ischemia. (B) Quantified infarct volumes expressed in percentage of the ischemic volume of the whole brain (ordinary one-way ANOVA, Tukey's multiple comparison test; (**)) adjusted p-value<0.01; F=8.75; R squared =0.77). (C) The quantified difference in hemisphere size relative to contralateral hemisphere by ordinary one-way ANOVA with Tukey's multiple comparison test. Significant difference of means was found with the (*) adjusted p-value<0.5; (***) adjusted p-value<0.001; F=7.34; R squared=0.27. Data is represented as mean±SEM.

Anatomical mouse brain referencing atlas from Allan brain map was utilized to map the regionality of the induced stroke. All strokes (n=16) were cortical with slight differences between the positioning of the ischemic area on the rostro-caudal axis. Even though a highly conserved branching point of the distal middle cerebral artery was consistently targeted during brain microsurgery, there are slight vasculature differences within each mouse which causes variation between stroke size and location. Affected regions are mainly confined between bregma positions 1.8 and -1.92 and the areas include the primary somatosensory area, supplementary somatosensory area, primary motor cortex and primary auditory area.

The infarct volume was at its maximum size on day 3 and then gradually reduced at each timepoint. By day 30, the infarct is significantly smaller, around 7% of the size on the infarct volume at day 3. Furthermore, swelling was observed immediately following stroke which persisted until day 3 of recovery. The ipsilateral hemisphere area increased by edema responses by 5.67% in comparison to the contralateral hemisphere. By day 7 the hemispheres were of similar size across all sample which indicated edema resolution. From day 10 up to 1-month succeeding cortical ischemia, the ipsilesional hemisphere was consistently smaller than the contralesional hemisphere. The tissue loss in the subacute phase of stroke recovery suggests loss of necrotic tissue and brain atrophy. (Sayed et al., 2020)

In figure 7a above, there is a dark violet stain observed within the infarct core on days 7, 10 and 30 post MCAO. The pattern of the darker staining is consistent with immune cell infiltration staining and later fibrotic scarring pattern. Therefore, the most probable cause is the CV solution binding to chromatin structures of the infiltrated and resident activated immune cells and stiff ECM. Furthermore, surrounding the increased signal is a visible zone of clear tissue indicating separation of infarcted and healthy parenchyma on days 7 and 10 post-induction of ischemia. On day 30, the clear zone becomes less apparent due to the clearance on necrotic tissue and contraction of the core within itself. Interestingly, at the late subacute timepoint, the condensed core seems to be slightly detached from the normal brain tissue on sections with the highest percentage of area affected. This might indicate some sort of spatial separation which the brain could utilize to protect itself from the possible neurotoxic effects of the robust fibrotic scarring on the healthy tissue.

3.1.2. Changes of the Infarct Core and Immediate Penumbra Region by Evaluation of Astrogliosis post-ischemia

Subsequently, we wanted to assess how the infarct core area changes over time post dMCAO in wt B6 mice. There are two distinct areas defined in stroke which are separated with robust glial limitans: The infarct core and the penumbra. The peri-infarct region or penumbra is characterized by astrocytes undergoing reactive astrogliosis identified with highly upregulated expression of the glial fibrillary acidic protein (GFAP). Since the astrocytes form a barrier between the necrotic tissue and normal parenchyma, the infarct core region is defined by the GFAP+ cellular margin. We quantified the infarct core areas of all MCAO and sham-operated mice (figure 8). Moreover, the morphological changes of astrocytes in the penumbra region are depicted and described for days 3, 7 and 30 post MCAO.

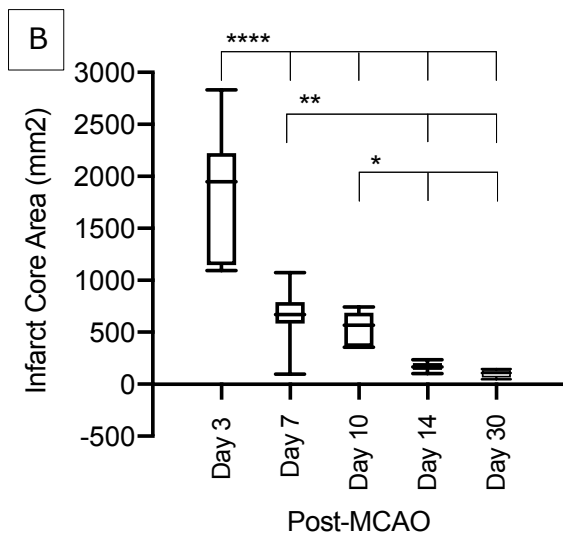
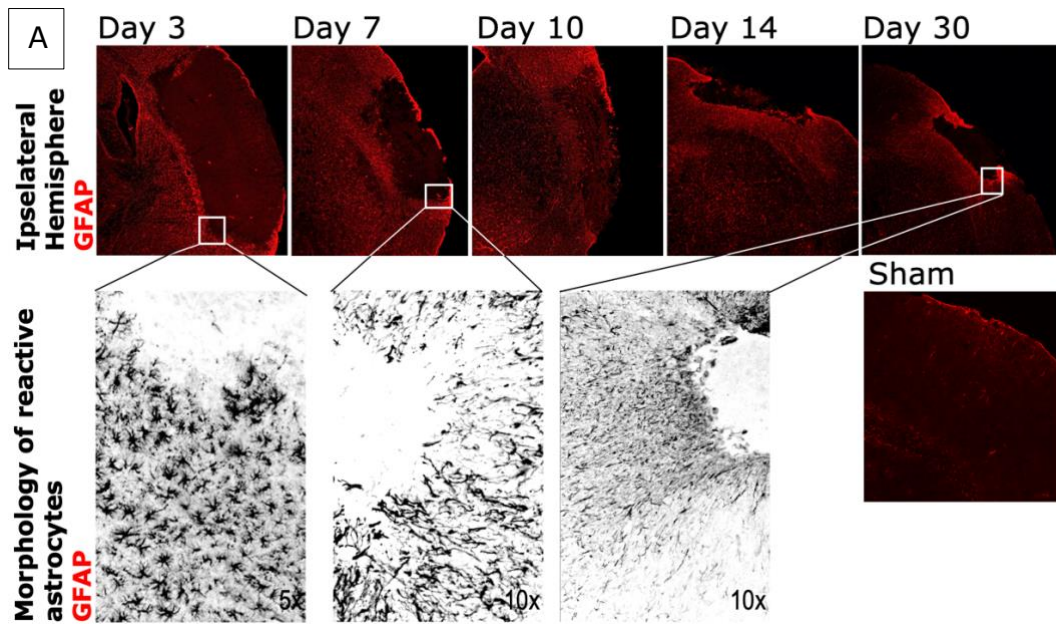


Figure 8. Infarct Core quantification defined by GFAP+ cellular margin and depiction of morphological changes of astrocytes. (A) Images of brain sections from infarct area of dMCAO operated mice. GFAP+ astrocytes at the site of injury are shown in fluorescent red on days 3, 7, 10, 14 and 30 post-ischemia. Sham-operated cortex is also shown with GFAP+ astrocytes present in the meninges and as part of the neurovascular unit in bright red. The second row depicts astrocyte morphology in acute and chronic phases of recovery. Astrocyte morphology is shown in black at the border between the infarct core and penumbra, where the representative image on day 3 is shown at 5x magnification, while day 7 and day 30 at 10x to better visualize the astrocytic protrusions. (B) Box and whisker plot of mean infarct core areas of a PLD timepoints. Significance

was determined by ordinary one-way ANOVA with a Tukey's multiple comparison test. (F=44.02; R squared=0.80; *p<0.05 **p<0.01 ***p<0.0001) Data is represented as mean±SEM.

As seen in figure 8a, by day 3 post MCAO the astrocytes display a stellate morphology with very high upregulation of GFAP expression compared to sham. We saw increased densities of astrocyte processes in the core border zone compared to the regions located further away. By day 7, the astrocytes retained their high expression of GFAP, but seem to extend their elongated processes toward the ischemic core. One month following the event, the streams of astrocyte processes in the peri-infarct area show a very robust barrier formation encapsulating the injured tissue. Furthermore, the assessment of the infarct core area changes through time shows that the necrotic tissue has the largest presence on day 3 and significantly decreases already 1 week after ischemia. The infarct core area gradually decreases further through the end of 1 month post recovery. Our results are consistent with the literature in several key aspects- morphological changes of astrocytes forming the glial scar, astrocytic spatial control indicated by various zonal densities and finally removal of necrotic tissue and closing of the infarct core area. Later timepoints will also be evaluated in the future to determine if the infarct core area stabilizes and persists for months/years after the event.

3.1.3. Fibrotic Response Evaluation by Col3 and ERTR7 IHC Through a Timecourse of 30 Days

To determine the rate of scar formation and pattern of ECM deposition, the infarct coronal brain sections were stained with Collagen 3 and ERTR7 fluorescently labelled antibodies. Collagen 3 is one of the main fibrillar collagens secreted within the 3D matrix, therefore it can provide us with insights on scaffold formation. ERTR7 is an unknown antigen found in the

cytoplasm of reticular fibroblasts however, through extensive usage of the antibody, it was observed that there is little to no distinction between various collagen and ERTR7 staining patterns.

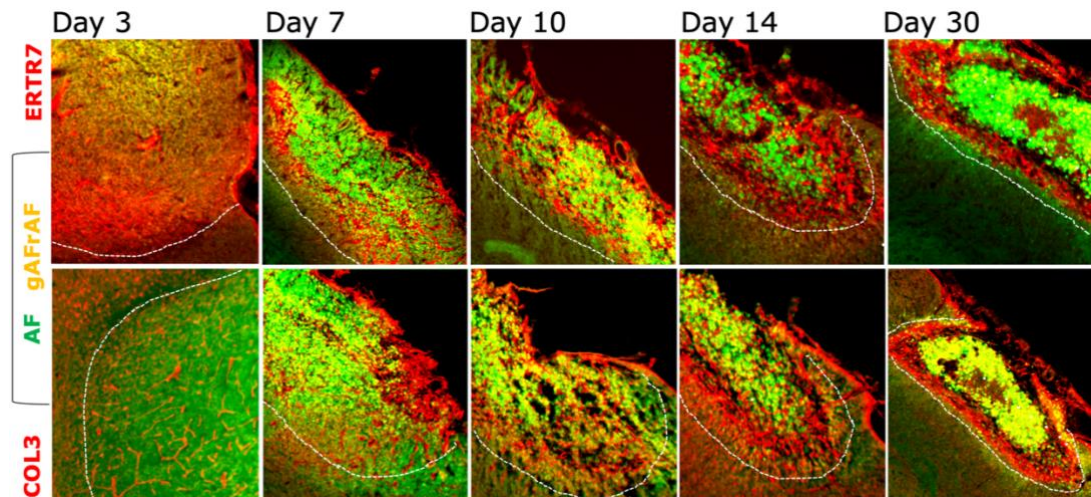


Figure 9. Collagen 3 and ERTR7 showing fibrotic scar formation in wt C57bl/6 mice in a period of 30 days post-ischemia. All images depict the infarct core area at 5x magnification. Top row shows ERTR7 staining in red and the bottom row depicts Col3 in red. Each column is a distinct PLD timepoint. All samples have exhibited very high levels of autofluorescence emission within the penumbra and peri-infarct areas at 400-600nm. Autofluorescence emitted through the whole spectral range is seen as bright green and yellow. Dotted line marks the border between the penumbra and infarct core defined by GFAP+ glial limitant.

Autofluorescence from tissue samples and specific antibody staining can be distinguished by the employment of spectral mixing. Since the auto fluorescent molecules exhibit a strong signal in both red and green channels, the overlap gives a yellow hue when imaged in both green and red channels Therefore specific staining from an Alexa fluorophore 594 is differentiated from autofluorescence by the lack of overlap with the green channel.

On day 3 post-ischemia, both ERTR7 and Col3 show upregulation of collagen surrounding the blood vessels in the core which is consistent with

the literature that describes the initiation of angiogenesis and neovascularization in subacute phases of stroke. (Munji et al., 2019) By day 7, the vascular collagen becomes less apparent and the staining patterns start to appear as deposited proteins mainly concentrated on the lateral portions of the scar and consistent with matrix morphology. By day 14 and 30, concentrated scarring is observed which seems to encapsulate the outer rim of the core, very close to the border with the glial scar. It could suggest that it serves as an additional barrier between the parenchyma and ischemic tissue. Therefore, we can visualize and delineate the timecourse of fibrotic scarring following ischemic stroke.

3.1.4. Preliminary Neuroinflammatory Response Evaluation by CD45 and IBA-1 IHC Through a Timecourse of 30 Days

We wanted to evaluate the preliminary neuroinflammatory response of the wt C57bl/6 mice following MCAO. The exact cell types involved as well as the timecourse of inflammation have been studied extensively following stroke. (Amruta, Rahman, Pinteaux, & Bix, 2020; Jayaraj, Azimullah, Beiram, Jalal, & Rosenberg, 2019; R. Liu et al., 2017) However, the basic analysis was carried out to determine the interaction of these cell populations with the developing fibrotic scar. Noticeably, 3 out of 35 mice were found with severe hydrocephalous at the time of tissue processing. Since the inbred strain is not described to commonly observe high rates of hydrocephalous, the anomaly is noted. CD45 was used as a broad marker for immune cell infiltration as many hematopoietic lineage cells are CD45 positive. Furthermore, to discriminate between various cells like macrophages/ monocytes and lymphocytes, the anti-Iba-1 (ionized calcium binding adaptor molecule 1) antibody was used which is found on infiltrating macrophages and local activated microglia.

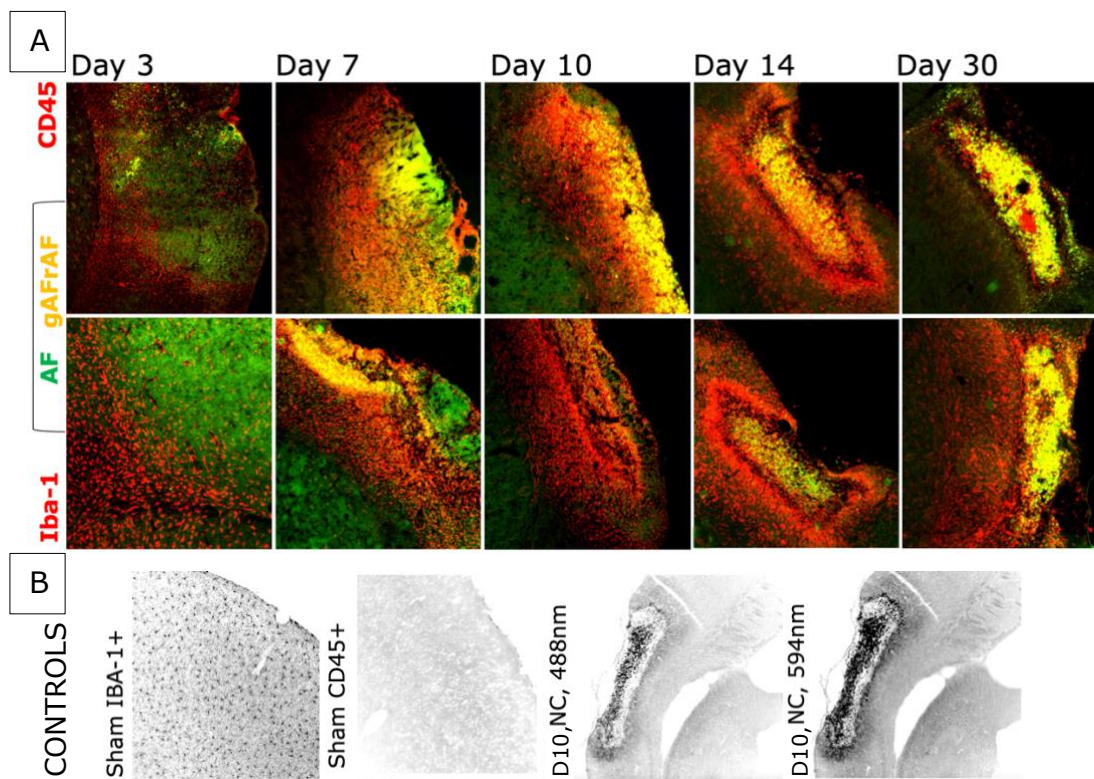


Figure 10. Neuroinflammatory response evaluated by IF of CD45 and Iba-1 wt C57bl/6 mice in a period of 30 days post-ischemia and the respective controls. All images depict the infarct core area at 5x magnification where each column is a distinct PLD timepoint. Top row shows CD45 staining in red and bottom row depicts Iba-1 in red. Autofluorescence is observed in all samples and channel 1 is seen as a green hue, while AF in the channel 2 is seen as yellow. (B) Controls for fibrosis and neuroinflammation evaluation where respective cortex of shams has been stained for CD45 and Iba-1. Also, d10 infarct core is shown displaying rigorous AF in 2 various channels. No primary or secondary antibodies have been added, but all other steps of staining have been carried out as described in methods section.

On days 3 and 7 post-ischemia, CD45 and Iba-1 show very similar cellular activation and the migration patterns observed in the penumbra and inner core with approximately over 80% overlap. According to various studies, the cellular population observed on both days are most likely infiltrating macrophages acting as mediators of neuroinflammation. (Buscemi, Price, Bezzi, & Hirt, 2019) On day 3, the CD45+ and Iba-1+ cells

appear to be distinctly separated from the most inner part of the core. Also, observing the whole affected cortex of all animals showed a possible migration pattern of CD45+ cells. The cellular population was seen on an axis from the thalamic nuclei to the site on the injury. To confirm the migration and directionality of movement, in the future we can utilize 2-photon live imaging.

Immediately following severe hypoxia, the resident microglia get activated, however, by day 3, macrophages are the main cell type found within the core. After day 7, the concentration of blood-derived macrophages starts to decrease, however, infiltrating T-cells are known to persist until day 14 post MCAO. (Feng et al., 2017) Furthermore, there could be an indication of spatial control by observing various densities of cells in the peri-infarct area on both days 10 and more pronounced, day 14. By day 30, there is almost full resolution of inflammation seen as the absence of CD45+ signal. However, the signal that is emitted is mostly present within the core itself. Finally, on day 30, Iba-1 is still observed but at a much lower cellular concentration, indicating persistent activated microglial populations. However, microglia are CD45^{low} (Rangaraju et al., 2018) which explains the absence of fluorescent emission of CD45+ on day 30.

As seen in figure 10b the lack of primary and secondary antibody addition revealed the very high levels of autofluorescence found at 400-600nm across all of our samples. The autofluorescence was limited to the infarct core and penumbra regions. The possible causes and ways how to eliminate them are discussed in section 4 below. Furthermore, sham-operated mice as well as the contralateral hemisphere of MCAO-operated mice have been used as controls for assessing appropriate staining, cellular morphology/location and surgery performance. Iba-1 staining in the shams were seen in resting microglia through both hemispheres, while immune cell infiltrates have not been seen in any of the cortexes of sham operated mice.

3.2. Single Cell RNA sequencing

3.2.1. FACS of GFP+ cells found within an ischemic infarct

We also wanted to assess the differences in transcriptomic expression of collagen producing cells within the infarct core. Col1GFP+ test mice were induced with dMCAO at 7 or 14 days after ischemia, subsequently the mice were euthanized, and their affected cortex was dissected and processed for fluorescence-activated cell sorting. The corresponding cortexes of control mice were also isolated to ensure a high enough cell count for droplet-based scRNAseq. An example of the acquired FACS plot of GFP+ cells can be seen below.

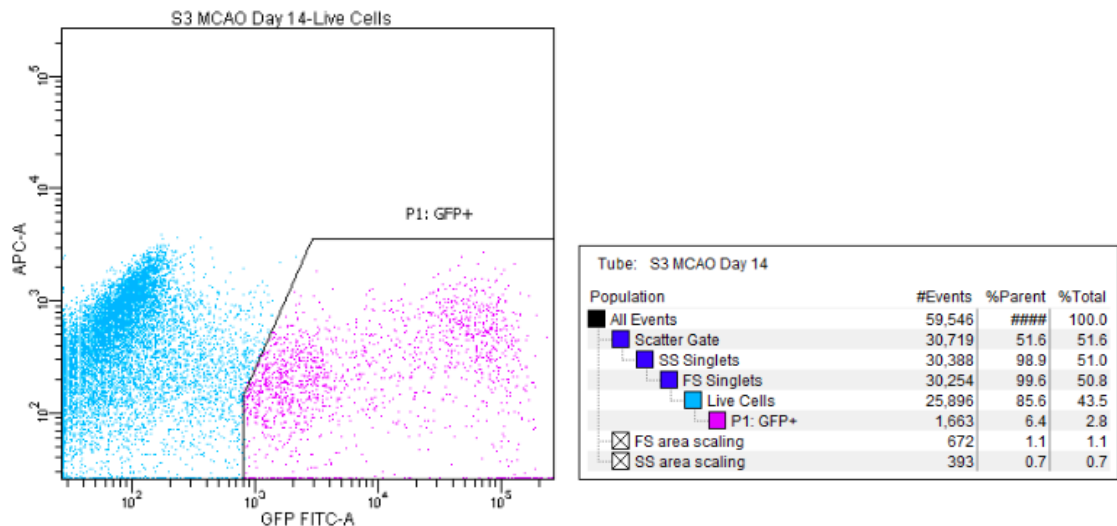


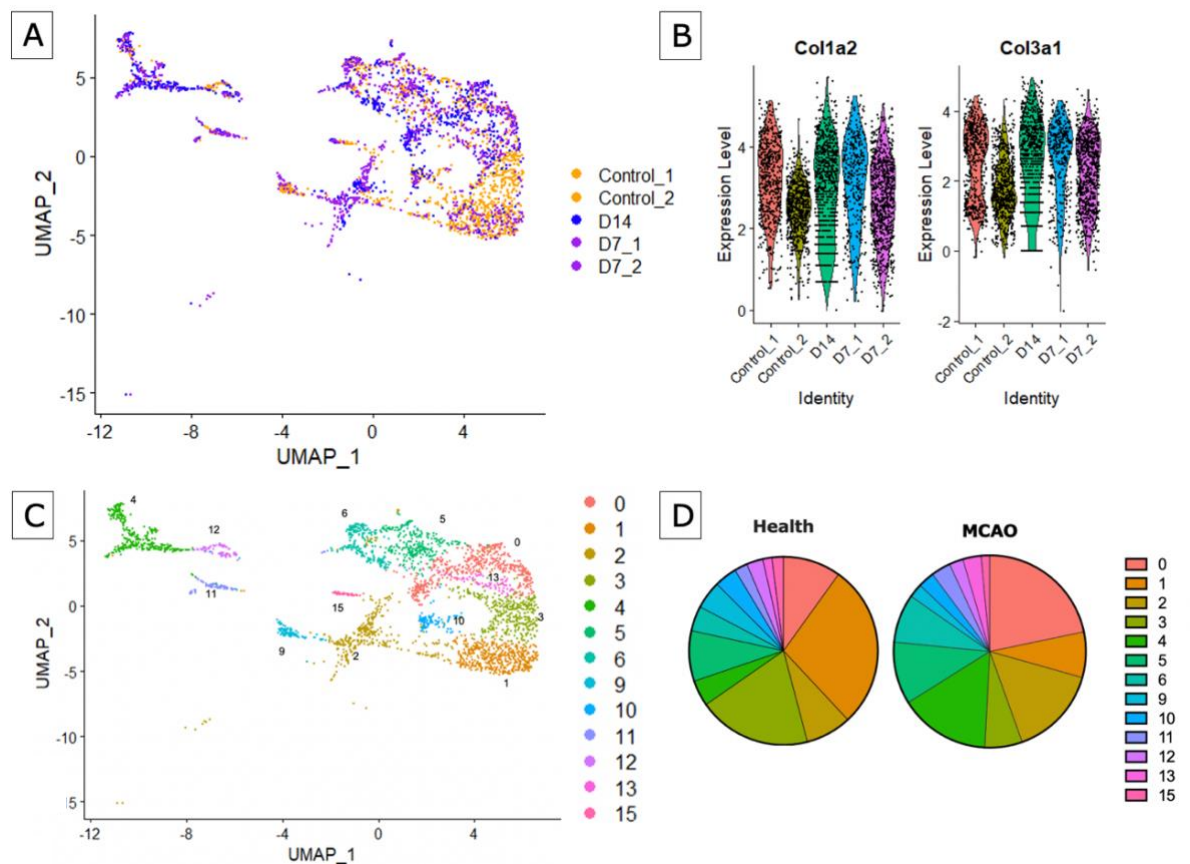
Figure 11. Flow cytometry analysis of live Col1GFP+ cells in the ischemic cortex of day 14 mice after permanent distal middle cerebral artery occlusion. Gating analysis reveals that from the total number of events, 1,663 of them are identified and separated as live GFP+ cells. In the cortexes of control mice, 728 and 289 cells were recognized and separated by FACS.

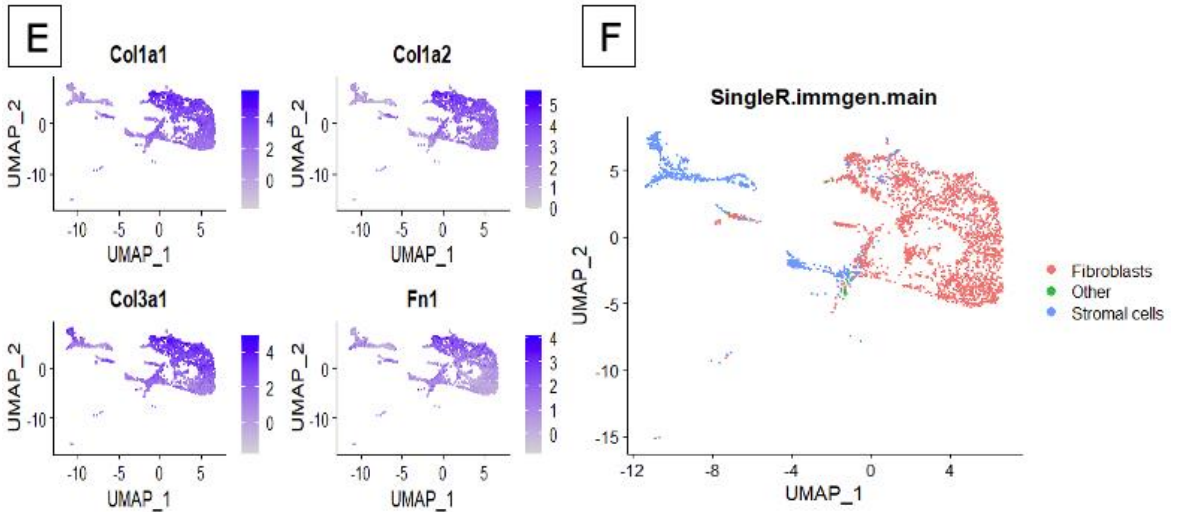
Since the pilot study revealed a very small number of Col1+ cells in a healthy cortex, both contra- and ipsilateral cortexes were isolated for this experiment. As all the graphs show similar patterns, therefore only the FACS plot of day 14 brain is depicted. Sorting of GFP+ cells from the

ischemic cortex on day 7 following dMCAO showed around 520 gated events.

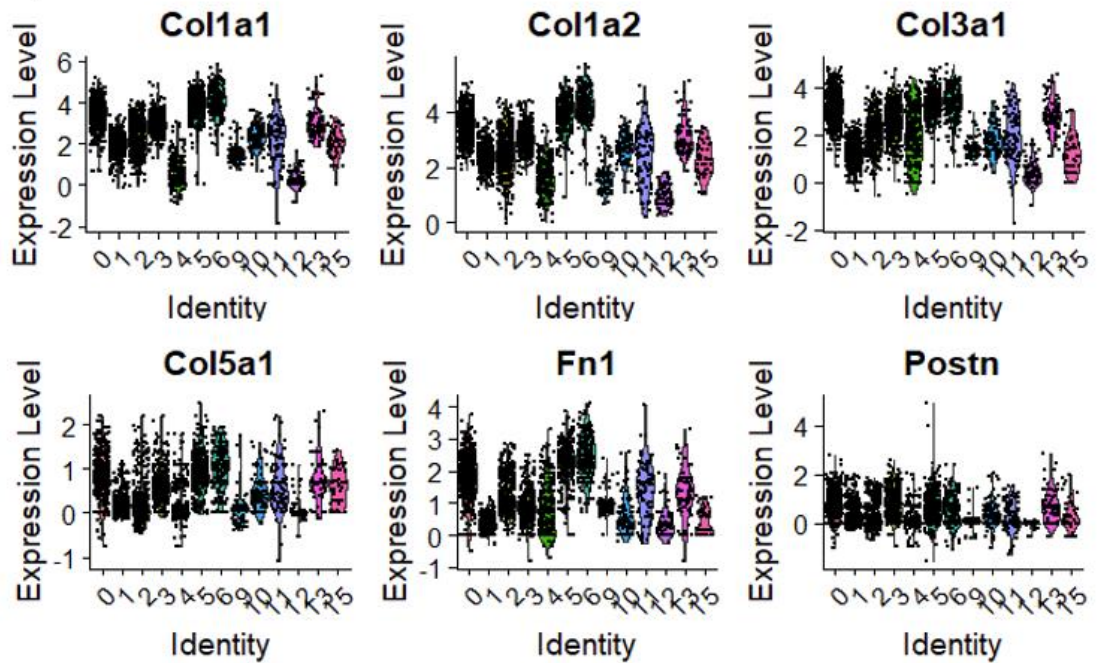
3.2.2. Transcriptional profile of scar forming cells post MCAO

To map the transcriptional profile of Col1GFP+ cells in health and following stroke, the FACS sorted cells were put through the droplet-based 10x Genomics pipeline as described in the methods section above. The data was run through Cell Ranger and Seurat v3.0 to filter and cluster the cells. One major and one minor class was observed, as seen in figure 12 below. The following results show us the transcriptomic variations between cells implicated in the fibrotic phase of stroke recovery, their most-probable cellular identities and the genetic expression of pathways implicated in fibrosis, inflammation and recovery.

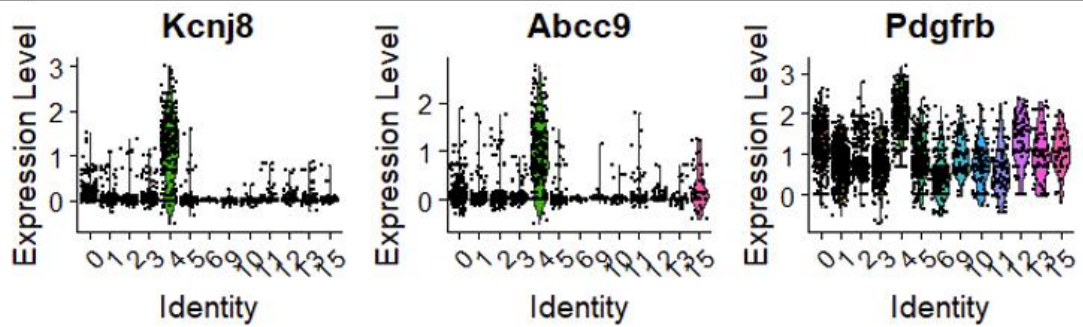




G COMMON GENES IN FIBROSIS



H PERICYTE COMMON MARKERKS



I VSMC COMMON MARKERKS

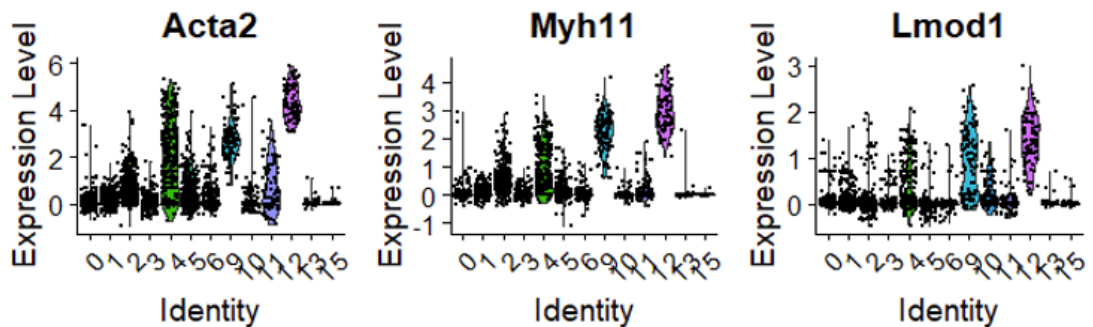


Figure 12. (A-I) Scar-forming cells have the transcriptional profile of fibroblasts at the single cell level and (G-I) the respective violin plots of the expression levels of pericyte, vSMC and fibroblast-specific genes per cluster. (A-F) Col1a1GFP+ cells from cortexes of healthy mice (n=2 samples with ipse-/contra side) and mice 5-7 days post dMCAO (day 7, n=2 samples; day 14, n=1 sample; ischemic cortex) were transcriptionally profiled at the single cell level and clustered using Seurat v3. A) UMAP plot with the sample identity (Health vs. dMCAO) labeled for each cell. B) Col1a2 and Col3a1 expression probability distributions across control and dMCAO samples 1. C) UMAP plot of the clustering analysis reveals 13 clusters that could be subdivided into two major classes: Class 1 (clusters 4,12 and 11) and Class 2 (cluster 0,1,2,3,5,6,9,10,12 and 15). D) Pie charts showing the percentage of each cluster relative to the total number of cells in health or d7/d14 dMCAO samples. (E) UMAP expression heatmaps of Col1a1- collagen 1 alpha 1, Col1a2 - collagen 1 alpha 2, Col3a1 - collagen 3 alpha 1 and Fn1 - fibronectin (F) UMAP plot with each cell labeled with its cellular identity determined using SingleR and the Immgen reference dataset (G) Fibroblast specific genes: Col1a1, Col1a2, Col3a1, Col5a1 - collagen 5 alpha 1, Fn1 and Postn - periostin. (H) Pericyte common markers: Knjc8- Potassium Inwardly Rectifying Channel J8, Abcc9 - encoding for sulfonylurea receptor 2 and PDGFRb - Platelet Derived Growth Factor Receptor Beta (I) vSMC common markers: Acta2 - smooth muscle alpha (α)-2 actin, Myh11 - Myosin Heavy Chain 11 and Lmod1 - Leiomodin 1.

Firstly, cluster analysis revealed that there are two primary clusters of cells which were defined and termed as 'major class', consisting of 9 separate clusters and as 'minor class', composed of 3 clusters, as seen in

figure 13, a and c above. The major class is composed of 2594 cells and the minor class of 516 cells. The distinct transcriptional profiles have been separated into 13 clusters and cellular identity was determined using SingleR, a computational method for unbiased cell type recognition of single-cell data sets using thousands of bulk RNAseq reference datasets from all organs. Whole gene expression analysis showed that the isolated cells are mainly fibroblasts and stromal cells. As seen in figure 12c and f above, the major class is composed of clusters 0, 1, 2, 3, 5, 6, 10 and 15 identified as fibroblasts, cluster 9 identified as vSMCs and other unidentified population of cells found in cluster 2. Stromal cells compose the minor class clusters 11, 12 and cluster 9 of the major class. These cells were determined to be pericytes (cluster 4) and vSMCs (clusters 9,11) and the expression plots of common markers are seen in figure 12h and i above. The expression heatmap of Col1a1, Col1a2, Col3a1 and Fn1 (figure 12e) shows that the major class mainly expresses genes implicated in fibrosis, but clusters 0, 5 and 6 consistently exhibit largest expression of aforementioned genes. Col3a1 is also being highly expressed in the cells found in cluster 4. Looking at the expression of collagen 1 and 3 per sample group (figure 12b), we can see that the GFP+ cells separated from the ischemic cortex on day 14, transcriptionally express Col1 and Col3 in a higher mean compared to all other samples.

In the UMAP plot showing sample identity, we can observe some separation of control and dMCAO samples. The control collagen producing cells are mostly concentrated in clusters 1, 3 and 9 (fibroblasts and vSMCs), and less abundant in clusters 5, 6 and 0, seen in yellow (figure 12a). Cluster 0, 5 and 6 comprise 74% of the stroke derived cells, while control cells are seen in very high percentage in clusters 1 and 3 with a third of cells being derived from stroke samples (figure 12d). Similarly, cluster 4 is also composed majorly of stroke samples with less than 16% of cells being derived from control samples. vSMCs clusters 9 and 11 have a similar amount of stroke and control samples (45% control).

Cells in clusters 5 and 6 are identified as fibroblasts in their activated myofibroblast-expressing phenotypic state. They seem to be the main drivers of scar formation in MCAO. This was determined by comparing expression levels of many fibrotic common marker genes, such as Col1, Col3, Col5, fibronectin and periostin between clusters in the major and minor class (figure 12h). Clusters 5, 6 and 0 located at the top portion of major class exhibit consistently high amount of gene expression for proteins forming the ECM scaffolds in the inner infarct. Analysis determined that clusters 1 and 3 have a consistent transcriptional profile with quiescent fibroblast cells. These clusters show less expression of proliferative and scar producing genes compared to activated fibroblasts. Furthermore, cluster 0 exhibits an intermediary phenotype between fibroblasts in clusters at the bottom versus top portion of the major class with an upregulation of collagen forming, ECM pathways, but not as severe as clusters 5 and 6. Cluster 1 and 3 exhibit similar expression profiles to fibroblasts in quiescence, and additionally have a preferential expression for Col15a1 and are therefore termed 'fibroblasts 1', in accordance with the classification provided by (Vanlandewijck, 2018), which used scRNAseq to classify vascular and perivascular cell populations in the mouse brain and found 2 population of fibroblasts. Cluster 15 did not show any preferential expression of ECM protein production genes, or pericyte/vSMC markers. However, preferential expression of Itga8 led to the hypothesis these fibroblasts could be identified as fibroblast 2 populations according to Vanlandewick classification. Since only one subset, fb1, was identified in our cluster analysis to have a role in ECM production, it could indicate that each subset might display distinct roles in the CNS during health and injury. Further analysis is needed to verify this observation.

We wanted to assess the percentage of each cluster relative to the total number of cells in health or d7/d14 dMCAO samples. The corresponding pie charts can be seen in figure 12d above. We can see that following MCAO, there is a higher percentage of activated fibroblasts (clusters 0, 5 and 6) then in health. Also, the pie charts show that there is a greater percentage of cells isolated from the control brains in the quiescent

state (clusters 1 and 3) then in stroke samples. This data could suggest that upon ischemia in the CNS, fibroblasts might get activated by various cellular and molecular mediators and undergo a transition where they induce upregulation of genes implicated in pathological fibrotic response.

The minor class includes clusters 4, 11 and 12 and were identified as stromal cells. The respective identities of each cluster were determined as pericytes (cluster 4) and vascular smooth muscle cells (vSMCs, cluster 9 and 11). Expression levels of *Knjc8* and *Abcc9*, pericyte-specific markers, seem to be exclusively expressed in cluster 4. Even though *PBGFRb* is expressed throughout all clusters, the highest mean expression is observed in the pericyte cluster 4, further confirming the cluster identity. Furthermore, pie charts in figure 12d above show pericyte populations increase in MCAO samples. Furthermore, the heatmap shows that a portion of cluster 4 upregulates genes needed for collagen 3 synthesis. This could imply that pericytes probably contribute to matrix formation in a lesser degree. Clusters 9 and 12 show expression patterns consistent with vSMCs – *Acta2*, *Lmod1* and *Myh11*. The increased transcriptional profile is almost mutually exclusive to clusters 9 and 12, except for pericytes showing upregulation of the aforementioned genes, however at a lower expression level.

No specific preferential transcriptional identity was observed in clusters 2, 10, 11 and 13. Unidentified cluster 2 also shows similar expression patterns of genes implicated in fibrosis as fibroblasts in quiescence, with the exception of fibronectin upregulation. Also, we can see that these cells are present in a higher percentage in MCAO samples compared to health.

This data suggests that fibroblasts undergo activation from a quiescent state when hypoxic conditions have injured the brain parenchyma. These activated fibroblasts show upregulation of genes implicated in the extracellular matrix formation. Together this indicates that fibroblasts seem to be the major contributors to ECM deposition, with pericytes and vSMCs displaying a minor role. To further discriminate between pathways or

patterns of activity of fibroblasts during health and MCAO, a heat map of scRNAseq transcriptome analysis for 61 genes is shown in figure 13 below. Preliminary analysis of the pathways and biological processes found to be preferentially expressed in activated fibroblast clusters will be performed with DAVID Bioinformatics Resources 6.8, NIAID/NIH and Reactome pathway mapping. The implications of the collected data are discussed in section 4 below.

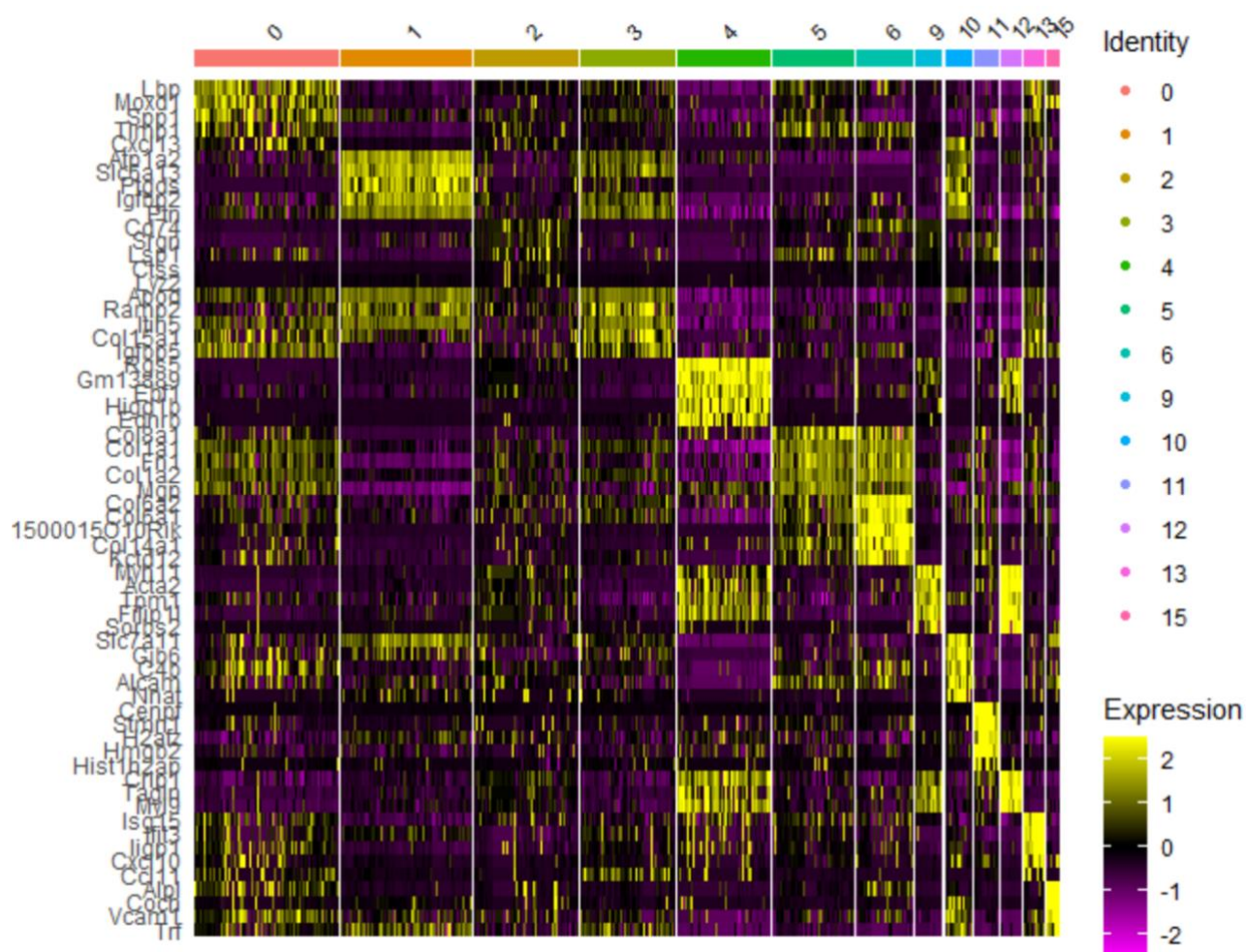


Figure 13. Heat map of the expression levels of the top 61 differentially expressed genes by Col1a1GFP+ cells from 7- and 14-days post dMCAO compared to Col1a1GFP+ cells from health. All cluster identities correspond with the color and number in results found in figure 12 above. (0- Fb Intermediary; 1,3- Quiescent Fb; 2,10,11,13- unknown; 4- pericyte, 5,6- Activated Fb; 9,11- vSMCs)

As we can see in the heat map, each cluster shows specific upregulation or downregulation of genetic expression. The full extended list of increased genetic expression has been utilized and processed with DAVID Bioinformatics Resources 6.8, NIAID/NIH and Reactome pathway mapping to determine which pathways and biological processes are driving gene expression in activated scar forming cells.

Firstly, we wanted to compare fibroblasts in a quiescent state (cluster 1 and 3) and activated state (cluster 0, 5 and 6). Analyzing genes upregulated in the respective cohorts shown in the heat map suggested which are the most significant pathways expressed in fibroblast post ischemia on days 7 and 14. The full list of the 25 most relevant upregulated pathways in activated fibroblasts determined by Reactome analysis can be seen in table 1 below. Upregulation of genes such as LBP (LPS binding protein), Cxcl13 (chemokine), Timp1 (MMP inhibitor) and others showed fibroblast involvement in the inflammatory immune response in the recovery phase post stroke. The preliminary pathway analysis showed that the GFP+ cells activated in the injured cortex upregulate transcriptional profiles which are mainly responsible in driving fibrosis, and secondly regulating the inflammatory response and supporting neurogenesis. Highest number of upregulated pathways are shown to be implicated in degradation of ECM matrix ($p=1.24E-11$), collagen chain trimerization ($p=3.98E-10$), ECM organization ($p=1.33E-7$), cell migration ($p=1.98E-4$), crosslinking of collagen fibrils ($p=1.85E-8$), elastic fiber formation ($p=1.09E-9$), NCAM1 interaction ($p=9.76E-6$) and many others which showed high expression selectivity for fibrotic scar formation genes. Moreover, looking at table 1 below we can see that signaling by PDGF ($p=7.19E-4$) was also shown to be driving the cellular response. PDGF is known to stimulate fibroblast proliferation and migration at the site of injury and is therefore most likely playing a role in the fibrotic scar response. (Rajkumar et al., 2006) Focal adhesion was shown to be stimulated by the FAK1/MET binding to integrins ($p=3.99E-5$). Very few downregulated pathways have been determined in activated fibroblasts, but the results did show high significance for genes

responsible for cholesterol metabolism ($p=8.83E-4$) and transport of fatty acids ($p=0.012$).

Table 1. 25 most relevant pathways that are implicated with genes upregulated in activated fibroblasts isolated by scRNAseq, sorted by p-value and determined by Reactome.

Pathway name	Entities				Reactions	
	found	ratio	p-value	FDR*	found	ratio
Assembly of collagen fibrils and other multimeric structures	28 / 67	0.005	1.11e-16	2.04e-14	24 / 26	0.002
Collagen formation	34 / 104	0.007	1.11e-16	2.04e-14	62 / 77	0.006
Degradation of the extracellular matrix	46 / 148	0.01	1.11e-16	2.04e-14	79 / 105	0.008
Collagen degradation	29 / 69	0.005	1.11e-16	2.04e-14	25 / 34	0.003
Extracellular matrix organization	73 / 330	0.022	1.11e-16	2.04e-14	230 / 319	0.024
Collagen chain trimerization	22 / 44	0.003	6.66e-16	1.02e-13	15 / 28	0.002
Collagen biosynthesis and modifying enzymes	26 / 76	0.005	1.07e-14	1.40e-12	38 / 51	0.004
ECM proteoglycans	24 / 79	0.005	1.32e-12	1.51e-10	13 / 23	0.002
Integrin cell surface interactions	25 / 87	0.006	1.48e-12	1.51e-10	27 / 55	0.004
Elastic fibre formation	16 / 46	0.003	1.09e-09	1.00e-07	16 / 17	0.001
Crosslinking of collagen fibrils	11 / 24	0.002	2.85e-08	2.37e-06	13 / 13	9.83e-04
Non-integrin membrane-ECM interactions	15 / 61	0.004	3.07e-07	2.33e-05	14 / 22	0.002
Molecules associated with elastic fibres	11 / 38	0.003	2.50e-06	1.77e-04	9 / 10	7.56e-04
Regulation of Insulin-like Growth Factor (IGF) transport and uptake by Insulin-like Growth Factor Binding Proteins (IGFBPs)	20 / 127	0.009	3.62e-06	2.24e-04	14 / 14	0.001
MET activates PTK2 signaling	10 / 32	0.002	3.67e-06	2.24e-04	5 / 5	3.78e-04
Signaling by PDGF	16 / 86	0.006	4.45e-06	2.54e-04	25 / 31	0.002
Anchoring fibril formation	7 / 15	0.001	8.51e-06	4.59e-04	4 / 4	3.02e-04
NCAM1 interactions	11 / 44	0.003	9.76e-06	4.98e-04	10 / 10	7.56e-04
Laminin interactions	9 / 31	0.002	1.98e-05	9.50e-04	14 / 15	0.001
Post-translational protein phosphorylation	17 / 109	0.007	2.15e-05	9.87e-04	1 / 1	7.56e-05
Platelet degranulation	19 / 137	0.009	3.51e-05	0.002	4 / 11	8.32e-04
MET promotes cell motility	10 / 45	0.003	6.49e-05	0.003	12 / 12	9.07e-04
Response to elevated platelet cytosolic Ca ²⁺	19 / 144	0.01	6.72e-05	0.003	4 / 14	0.001
Syndecan interactions	8 / 29	0.002	8.07e-05	0.003	9 / 15	0.001
NCAM signaling for neurite out-growth	12 / 70	0.005	1.44e-04	0.005	21 / 23	0.002

<https://reactome.org/PathwayBrowser/#/ANALYSIS=MjAyMTAxMjQxOTM1NTIlfNTc1NA%3D%3D>

Following Reactome analysis, we used DAVID for analysis of the full enriched gene list in activated clusters. The input gene list included all upregulated genes identified in activated clusters 0, 5 and 6 by single cell sequencing. The output information concerning the significant biological process found to be preferentially expressed are mostly the same as determined by Reactome involved in ECM formation and organization. The extended list did show a couple of additional processes that were implicated with very high significance such as angiogenesis ($p=1.1E-9$), wound healing ($p=2.48E-8$), positive and negative regulation of cellular migration ($p=6.6E-8$), axon guidance ($p=9.6E-7$), collagen catabolism ($p=4.5E-6$) and more. In addition to Reactome data displayed and described above, Kegg_Pathway analysis showed that activated fibroblasts could potentially regulate their cell cycle during ischemia by PI3-AKT signaling ($p=6E-10$). Growth factors bind to receptor tyrosine kinases which activates IRS1 stimulating a variety of gene expression. All of the mentioned proteins and their receptors were found upregulated in activated fibroblasts. Furthermore, focal adhesion and cell migration were identified to be stimulated by $\alpha 1\beta 1$ integrin binding to the ECM matrix which in turn activates and recruits FAK1 (also known as PTK2). Recruitment activates PI3-AKT, which in addition to regulating the cell cycle is also known to be involved in cellular migration and adhesion. 28 genes have been recognized within the pathway. Lastly, pathway analysis revealed that the activated fibroblasts could upregulate gene expression which drives neurogenesis and axonal sprouting. IGFs and IGFBP1 and 2 have been upregulated in activated fibroblasts which might imply certain neuroprotective mechanism of the fibroblasts found within the core. This preliminary analysis of possible molecular mechanisms and potential roles of the scar producing cells post ischemia shows that fibroblasts could have a protective phenotype after extensive cortical injury.

Furthermore, analyzing vSMCs and pericytes cluster specific gene expression also showed specific pathway selectivity. The low number of genes was found upregulated in the clusters, however smooth muscle contractions ($p=2.57E-7$) and NOTCH signaling ($p=3.23E-4$) were significantly upregulated in the respective cellular populations.

3.3. Recovery Implications of Fibrotic scarring

To evaluate how fibrotic scar formation impacts motor recovery following MCAO, thymidine kinase was utilized in combination with selective expression of CreERT to ablate dividing cells which produce collagen 1 at rest, following the administration of ganciclovir, and thus reducing the fibrotic scar formation. By evaluating the differences in motor recovery of mice expressing the Col1a2CreERT2+HTK (Test) and HTK (Control) following ischemia, it is possible to determine whether the ECM matrix and the cells that deposit it have neuroprotective or a neurotoxic effect during recovery. We used the adhesive tape test to assess differences in sensorimotor deficits in test and control mice. First, all test and control mice were acclimated, habituated and pre-trained for 3 days prior to micro neurosurgery. The baseline was evaluated on day 0 to evaluate if the cohorts exhibited an asymmetrical preference to the right or left paw. The ratio of preference in both cohorts was 0.9 with a slight favor toward the ipsilateral (left) paw. The mice were tested on days 3, 7, 14, 21 and 30 days following MCAO. On day 30, the mice were euthanized and perfused for following tissue analysis. The 2 cohorts will be examined for disparities between the overall infarct volume, infarct core volume, neuroinflammatory response and reactive astrogliosis. The information on the severity of sensorimotor deficits together with the histological findings will provide certain insights on the phenotypic expression of the scar. The whole experimental procedure and the subsequent evaluation is performed blinded. Unfortunately, due to the extensive time needed to perform the histological evaluations, only the assessment of motor recovery has been analyzed and shown in the thesis. Future evaluation of the stored brains will be needed to confirm the phenotype exhibited and shown in figure 14 below.

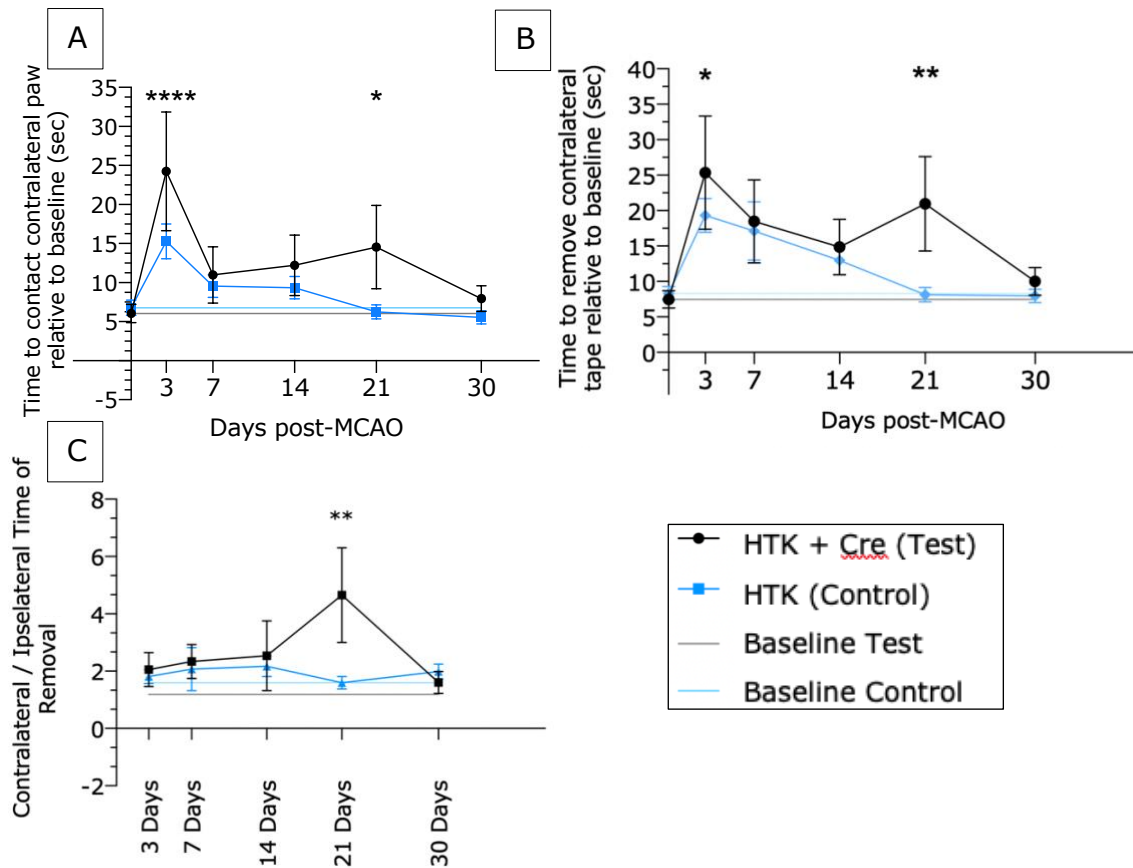


Figure 14. Adhesive Tape Test evaluation of limb function post stroke where (A) depicts the time to remove the tape from the contralateral paw compared to its baseline and control performance. Significance was determined with two-way ANOVA with Tukey's multiple comparison test. (B) Time of contact of the contralateral paw of test and control mice. Significance was determined with two-way ANOVA with Tukey's multiple comparison test. In (C) the ratio of contralateral/ipsilateral function relative to their baseline has been shown. Significance was determined with two-way ANOVA with Sidak's multiple comparison test (* $p < 0.05$; ** $p < 0.01$; **** $p < 0.0001$). In all graphs the test cohort is shown in black with its baseline assessment presented with a grey line. The control cohort and its baseline are seen as blue and light blue lines. Data is represented as mean \pm SEM.

During the subacute phase of stroke recovery on day 3, the time needed to remove (TOR) and contact (TOC) the adhesive strip on the contralateral paw in test mice was significantly higher compared to its

baseline assessment ($p < 0.0001$). Furthermore, it took the test mice for TOC of contralateral paw significantly longer compared to the control ($*p = 0.02$) cohort. There was no statistical significance between test and control mice for the time needed to remove the tape found on the left paw ($p = 0.65$) on day 3. However, a trend was observed where control animals show consistently shorter times needed for TOR and TOC on the affected paw compared to the test cohort. dMCAO has been induced in the right cortex and the affected areas include the primary motor cortex, primary and supplementary motor cortex. Since the right hemisphere controls the left side of the body, the contralateral paw showed deficits. After day 3, the control mice exhibit decreased times for TOR and TOC in each consequential trial, reaching the equivalent time to execute the task as their baseline performance on day 21. However, in mice where the fibrotic scar producing cells have been ablated, we can see that the test mice perform the task statistically significantly longer compared to the control TOR contra/ipse and test TOR baseline, as well as Test TOC ipse and control TOC contra/ipse. This is a very interesting and unexpected result as a detrimental role was contributed to fibrosis in the CNS. This could indicate that the fibrotic scar post-ischemia could have a neuroprotective phenotype. It suggests that the scar formation, clearance of necrotic tissue and finally forming of robust glial and fibrotic limitants separating the tissue from the parenchyma might be acting beneficially to the tissue. What other functions of collagen producing cells might be attributed to these effects?

To assess if certain asymmetry in responses resulted in such findings, we analyzed the TOR contralateral/ipsilateral plot over time. In figure c above, the dramatic increases in the mean time of test animals to perform dexterous paw movements and remove the tape on the affected paw is further illustrated. The mean difference of test and control performance is 3.1 seconds (95CL=0.67 to 5.45; $p = 0.0019$). To be able to verify the validity of findings, it is crucial to firstly histologically assess the cohort brains. Also, this experiment will be repeated in the future to determine whether this is a reproducible and consistent observation and thus has merit.

4. Discussion/Outlook

To determine the rate of scar formation, the pattern of ECM deposition, the role of the scar during recovery and potential molecular mechanisms that drive fibrosis in CNS, it is necessary to have a reproducible method to induce ischemia in a model organism. We used distal MCAO microsurgery with a 60-minute clamping time of the ipsilateral CCA for all experimental models in this study. To have valid results, we also had to provide evidence that the ischemic event has been performed adequately and that the ischemic cascade occurred according to current knowledge found in the literature. We have validated our procedure by evaluating the cortical regionality, total brain volume affected, hemisphere asymmetry, and finally the neuroinflammatory and astroglial response.

All strokes were cortical where the main areas affected are the primary somatosensory area, supplementary somatosensory area, primary motor cortex and primary auditory area. There are minor differences between positioning of the infarct on the rostro-caudal axis due to slight vasculature differences within each mouse which causes variation between stroke size and location. In this study, we used the adhesive tape test to assess motor recovery post MCAO, however evaluating cortical regionality of dozens of microsurgeries performed in the last year can give us better insight into optimizing our behavioral testing of rodents. Since the auditory cortex has been affected in a large portion of the animals, tests such as evaluation of task performance in sound-attenuating behavioral chambers can be used in the future (O'Sullivan, Weible, & Wehr, 2019).

Furthermore, we wanted to define the specific timing of tissue loss, contraction and cortical atrophy. In all dMCAO operated mice, edema of the ipsilateral hemisphere was seen on day 3, followed by resolution on day 7. From day 10 post dMCAO until day 30 we saw that the ipsilateral hemisphere was consistently smaller compared to the contralesional hemisphere suggesting cortical atrophy. A variety of inflammatory responses are likely to be responsible for such observations such as initial

upregulation of MMPs, leukocyte adhesion molecules, various cytokines, chemokines and many other pro-inflammatory mediators, followed by activation of resident microglia and infiltrating macrophages phagocytosing debris and necrotic tissue. The presence of such cells was also shown by CD45 and Iba-1 staining of brains on days 3, 7, 10, 14 and 30 post dMCAO. (figure 10.) According to the literature, CD45+ mast cells are known to be concentrated in the perivascular regions of the thalamic nuclei and have been implicated to exacerbate CNS damage in models of ischemia by contributing to BBB damage and swelling. (Goldschmidt, Hough, & Glick, 1985; Parrella, Porrini, Benarese, & Pizzi, 2019; Silverman, Sutherland, Wilhelm, & Silver, 2000) We have observed CD45+ cellular axis from the thalamic nuclei in the subacute phase of recovery post ischemia. To confirm migration directionality, we can use live imaging techniques. The resident microglia and infiltrating macrophages get activated and further upregulate pro-inflammatory signals. Furthermore, spatial control of immune cells was observed as increased fluorescence immediately surrounding the infarct core and lower densities of cells seen in the peri-infarct areas on both days 10 and more pronounced, day 14 (figure 10.). By day 30, there is almost full resolution of inflammation seen as the absence of CD45+ signal. Additional experiments analyzing neutrophils, lymphocytes and other immune cells is necessary to further understand how each of these immune cells is interacting with the fibrotic scar. We will then look at the brain section where the fibrotic scar has been ablation and assess if immune cell numbers, or localization of immune cells changes.

Since the ischemic response closely correlates with the pattern observed in most publications, it was concluded that all of the quantified microsurgical procedures have been performed adequately and more importantly, consistently. Furthermore, all sham operated mice observed no fibrotic or inflammatory response evaluated by antibody staining with Col3, ERTR7, CD45 and Iba-1.

Astroglioses following an ischemic event has been extensively studied throughout the years. It was shown that astrocytes initially react at 24-48

hours post MCAO with distinct hypertrophic morphology and later form into scar forming cells which provide a border with the inflamed tissue from the rest of the parenchyma. (Buscemi et al., 2019; Ding, 2014; Morizawa et al., 2017) This was confirmed in this study by GFAP immunofluorescence staining. On day 3 we saw high GFAP expression and stellate astrocyte morphology located mainly in the infarct penumbra. By day 7, the astrocytes retained their high expression of GFAP, but seem to extend their elongated processes toward the ischemic core. (figure 8) This is also one of the commonly known properties of the astroglial scar. (Buscemi et al., 2019) A clear glial limitant was formed by day 30 which was already shown to have a dual role in the CNS post ischemia. It confines the inflammation to the core however, it also serves as a barrier to regenerating neurons and sprouting axons. Since the GFAP+ cellular margin defines the border of ischemic inner core, quantification of the core area also provided insights into the timing of contraction of the core. The inner core had the largest size on day 3 after ischemia and decreased by more than double already 4 days later. The area gradually decreases further through the end of 1 month of recovery. In the future, we plan to evaluate the infarct core volume changes up to 6 months of recovery. This will provide us with the information on whether the ECM scaffolding persists in the brain or is eventually cleared by immune and glial cells in the CNS following cortical ischemia.

In this study, we wanted to describe the fibrotic response in detail in a 1-month period following ischemia in mice. As seen in figure 9, on day 3, ERTR7 and Col3 co-stain with CD31, an endothelial cell marker, indicating upregulation of vascular collagen. This is consistent with angiogenesis and neovascularization in subacute phases of stroke. By day 7, the vascular collagen becomes less apparent and the staining patterns start to appear as deposited proteins mainly concentrated on the lateral portions of the scar and consistent with matrix morphology. By day 14, concentrated scarring is observed which seems to encapsulate the outer rim of the core, very close to the border with the glial scar. By day 21 very robust scarring on the lateral portions of the inner core is seen which persists until day 30 post

ischemia. In the future the timecourse will be expanded to further evaluation at 2, 3 and 6-months of recovery following dMCAO. The persistent concentrated scarring encapsulating the medial portion of the core could suggest that it might serve as an additional barrier limiting inflammation between the parenchyma and ischemic tissue. Even though scientists have hypothesized the possible function of the fibrotic scar tissue, it is unknown if this scar serves a similar role to astrogliosis or if there a novel, previously undescribed role. Moreover, on day 14 the protein fragments seem to be more scattered and disorganized on the formed border as well as in the middle of the core compared to day 30. This could signify some sort of intended spatial organization with a specific function. The robust ECM scaffold is the most probable cause of the injured tissue slightly dissociating from the CNS observed across all samples in the late chronic timepoint.

Initially, we wanted to test for the presence of various ECM proteins including various fibrillar and non-fibrillar collagens, fibronectin, laminins, elastin and others. There was very high autofluorescence present in the core itself, which made discriminating between the immunofluorescence of secondary antibodies and the autofluorescent signal very challenging. Control samples showed that our core fluoresces in a range of excitation 330-500nm and emission 400-700nm in wavelength, and we hypothesize that intracellular and extracellular fibrous proteins are partially responsible, as the emission range of the fibrotic biological constituents is between 400-510nm. Moreover, the emission signal is also present at longer wavelengths in the red channel which covers the spectral range of 590 to 650nm. Evaluating the morphology of the autofluorescent signal gave insight that our second molecule likely to cause such high emission is lipofuscin. Lipofuscin molecules are pigments that accumulate in postmitotic cells such as neurons and have been implicated as a hallmark of aging. (Moreno-García, Kun, Calero, Medina, & Calero, 2018) Various studies also use the presence of lipofuscins to demark the area of infarction. (Chung et al., 2018) In the future, we plan to use CuSO₄ in ammonium acetate buffer or 1% Sudan Black B in 70% ethanol to reduce or eliminate lipofuscin

autofluorescence in paraformaldehyde fixated mouse sections. (Schnell, Staines, & Wessendorf, 1999) Furthermore, we will avoid using Alexa fluorophore 488 to circumvent the autofluorescence of fibrous proteins in the ischemic cortex. The combination of these two techniques will hopefully yield decreased or eliminated autofluorescence which should allow us to stain for various other fibrous and immune cell markers to further characterize infarct core scarring.

Furthermore, to gain certain insight into the function of the fibrotic scar, we utilized genetic recombination of a thymidine kinase with cell specific targeting by CreERT to induce ablation of scar producing cells in a specific timeframe. Since thymidine kinase activates the administered prodrug ganciclovir to become cytotoxic to dividing cells, it allows for temporal control for ablating proliferating collagen producing cells. As described in figure 14, the control cohort showed a consistently shorter time needed to contact and remove the strip from the contralateral and ipsilateral paw. However, a statistically significant result was observed on day 21, where the test mice showed a dramatic increase of time needed to both contact and remove the tape from the affected paw. This could suggest that the fibrotic scar found in the ischemic cortex of mice acts in a protective manner towards motor recovery in the weeks following MCAO. Previously, it has been hypothesized that the fibrotic scar acts in detriment to the CNS due to the high ECM matrix content potentially limiting brain plasticity needed for learning and memory throughout life. However, our findings show contradicting results. Studies have shown that ablating stromal cells following spinal cord injury results in failure to seal the injured tissue. (Göritz et al., 2011b) The resulting increased inflammation response and absence of tissue integrity stabilization could explain our observations. Therefore, it is of importance to repeat the HTK experimental procedure and to perform immunohistochemistry on the tissue to confirm our findings are reproducible and lead to valid conclusions. We speculate that in the absence of scar producing cells, there is increased immune cell infiltration which persists until subacute phases of stroke providing more damage to the tissue mediated by proinflammatory signals. Furthermore, we hypothesize

that the core does not contract within itself which leads to increases injured area. Finally, we think that there is decreased neurogenesis and glial recovery in the ischemic penumbra in the absence of scar producing cells. We have used a specific Col1a2CreERT mouse line to label the cells that produce col1a2 at rest. Previously we have found these to be primarily fibroblasts and since in the scRNAseq data there is some evidence that pericytes also turn on collagen expression, we may not have completely gotten rid of the fibrotic scar. Further verification is necessary.

This observation of decreased motor recovery in the absence of fibrotic scarring leads to a plethora of new questions concerning the fibrotic scar. Firstly, on day 30 post dMCAO, we saw that the performance of both test and control mice reached close to their baseline performance. Therefore, the translation of motor recovery in humans post stroke will have to be further examined. Also, the exact molecular mechanisms that lead to the fibrotic formation on day 21 need to be evaluated to determine how this response affects various vascular, glial and neuronal cells post ischemia. We also want to perform single cell RNA sequencing of brains affected by ischemia with the same HTK+Col1a2CreERT genotype to examine the differences in transcriptional profiles of cell types in and surrounding the infarct with and without the presence of collagen producing cells. All of these future experiments will give us a much greater understanding of the role and implications of fibrosis post ischemia. Due to the severe translational failure of basic research to stroke clinical trials, it is necessary to gain a more comprehensive understanding of all components of the ischemic response. Every week, new publications arise showing decreased infarct size and better recovery post stroke implicated by targeting singular aspects of the ischemic cascade. However, no new therapeutic options have been provided to millions of people worldwide affected by stroke since 1996, with the approval of recombinant tissue plasminogen activator or rTPA. Even though the problem nor the situation is simple and incorporates many issues, each new insight into the pathological mechanisms following ischemia in the CNS brings the scientific community closer to the answer. Could the answer be the fibrotic scarring found in the infarct core area?

Hopefully, our future experiments will provide a more definitive answer. Acquiring this preliminary data led us to a new hypothesis concerning the potential mechanisms that aid in better recovery.

In the last performed experimental procedure, we have utilized scRNA sequencing to assess the differences in transcriptomic expression of collagen producing cells within the infarct core. The fibrotic response has been studied extensively in the periphery; however very little importance was given to understanding the scarring post ischemia in the CNS. Our results lead to the conclusion that there is clustering of fibroblasts in health versus stroke. The data suggests that following ischemia in the CNS, fibroblasts are transiting from a quiescent state to an activated state with increased enrichment of genes implicated in fibrosis. MCAO samples used for scRNA analysis, show a much higher percentage of activated fibroblasts compared to health and lower percentage of fibroblasts in quiescence. The activated fibroblasts exhibit higher expression levels of extracellular matrix genes compared to fibroblasts in the quiescent state. Finally, fibroblasts seem to be the major contributors to ECM deposition, with pericytes and vSMCs displaying a minor role. Previously, various cell types such as pericytes were hypothesized to be the major cellular players in fibrosis in the CNS. (Göritz et al., 2011b; Shibahara et al., 2020) A problem in the field is lack of marker specificity and therefore distinction of cell of interest can be easily mistaken. Our study shows that cells with the transcriptional profile of fibroblasts are the main contributors to the ECM formation.

Subsequently, pathway analysis with Reactome and DAVID software revealed specific upregulated cellular pathways of activated fibroblasts. The majority of upregulated gene expression is implicated in cellular migration, adhesion and extracellular matrix formation and organization. Moreover, it was shown that post MCAO, activated fibroblasts activate cellular migration and regulate their cell cycle by PI3-AKT signaling and/or PDGF signaling. These pathways could be used in the future to manipulate fibrosis post ischemia into a more protective phenotype. Furthermore, activated fibroblasts showed to upregulate gene expression which could potentially

drive neurogenesis and axonal sprouting. In the CNS, IGF1 signaling plays a role in neuronal survival, neurite outgrowth and myelination in homeostasis and injury (Bondy, Cheng, Zhong, & Lee, 2006). Post-ischemia, IGFs have been shown to reduce neuronal loss and increase glial proliferation (Lewitt & Boyd, 2019). IGFs and IGFBP1 and 2 have been upregulated in activated fibroblasts which might imply certain neuroprotective mechanisms of the fibroblasts found within the core. This preliminary analysis of possible molecular mechanisms and potential roles of the scar producing cells post ischemia shows that fibroblasts could have a potential neuroprotective phenotype after extensive cortical injury. This newly formed hypothesis has also been validated by statistical evaluation of sensorimotor recovery post stroke described previously.

Furthermore, three clusters could not have been identified through common expression patterns. However, close transcriptional profile analysis did provide insight into the possible identity of cluster 11. Unidentified cluster 11 does show slight upregulation of *Acta2*, however the cluster does not show upregulation of other common vSMC or pericyte markers. Importantly, cluster 11 does express ECM specific genes. An important insight into the cluster identity could be the *RGS5* gene, upregulated in pericyte cluster 4. *RGS5* is responsible for the migration of pericytes from the perivascular spaces into the parenchyma site of injury which is ultimately thought to lead to transdifferentiation and induction of fibroblast-specific genes. Therefore, cluster 11 could be pericytes and/or vSMC populations that have migrated to the ischemic core and initiated transcription of ECM producing genes. Studies have shown that *RGS5*-KO mice do not show statistically significant differences in the amount of ECM in the fibrotic scar post MCAO (Roth et al., 2020), therefore the cluster should not impact the evaluation of the main fibrotic response pathways.

4.1. Conclusion

To conclude, we wanted to answer several questions concerning fibrotic scar formation following ischemia in the CNS previously undescribed in the literature. First, we wanted to define the timecourse of scarring in response to ischemia in the CNS. We saw initial upregulation of vascular collagen and by day 7 there was visualisation of initial matrix formation. By day 14, a tough ECM matrix was observed that encompassed the whole core. It was present at day 30 with no significant ECM protein clearance. The core seemed to be stabilized forming a separation border with the rest of the parenchyma. Furthermore, in the future we also plan to assess whether the scar persists permanently post-ischemia and define the presence of all major biological constituents in the core.

Secondly, we wanted to determine which cells are the main contributors of ECM deposition. Using single cell RNA sequencing, we have provided evidence that cells with the transcriptional profile of fibroblasts are mainly responsible for extracellular matrix organization in the core of an ischemic cortex, with pericytes and vSMCs displaying a minor role. Also, our data suggests that fibroblasts get activated following ischemic injury turning on the expression of scar producing genes. Lineage tracing will be performed in the future to determine the origin of collagen-producing cells. To determine if scar-forming cells originate from pericyte transdifferentiation or the proliferation of resident CNS fibroblasts, we will perform lineage tracing experiments using CreERT lines that label each cell type. NG2CreERT2 will be used to label pericytes, and Col1a2CreERT mice will be used to label the small, resident population of CNS fibroblasts. Our preliminary data leads to the hypothesis that resident fibroblasts get activated by a variety of signals and induce differential gene transcription to drive the fibrotic response to injury. Additionally, we wanted to see what molecular mechanisms drive fibrosis in the CNS post ischemia. Pathway analysis of gene upregulation of activated fibroblast clusters identified by scRNAseq showed mainly transcriptional profile of protein expression responsible for ECM scaffold formation, immune response stimulation and

pathways that drive axonal sprouting and neurogenesis. More stringent analysis will be performed which will provide the understanding of specific cellular and molecular players driving the fibrotic response.

Lastly, we have asked ourselves how the scar tissue is implicated in recovery. Preliminary results showed that the scar appears to be neuroprotective during motor recovery assessment. This unique result has to be repeated and histological analysis has to be carried out to determine whether scar forming cells have indeed been ablated. Also, specific immune response differences of test and control cohorts will be further examined.

Finally, we also want to perform corresponding fibrotic scar evaluations in female mice since only male mice have been used in this study to limit outcome variability. Sexual dimorphism in stroke patients has been observed and described in humans and model organisms alike. A better understanding of fibrosis post ischemia in males and females can lead to manipulation of cellular pathways that show to be neuroprotective or neurotoxic to the recovering CNS. This could provide us with better therapeutic options in the future for stroke patients worldwide.

5. Literature

- Amruta, N., Rahman, A. A., Pinteaux, E., & Bix, G. (2020). Neuroinflammation and fibrosis in stroke: The good, the bad and the ugly. *J Neuroimmunol*, *346*, 577318. doi:10.1016/j.jneuroim.2020.577318
- Arseni, L., Lombardi, A., & Orioli, D. (2018). From Structure to Phenotype: Impact of Collagen Alterations on Human Health. *International Journal of Molecular Sciences*, *19*(5). doi:10.3390/ijms19051407
- Bachem, M. G., Schünemann, M., Ramadani, M., Siech, M., Beger, H., Buck, A., . . . Adler, G. (2005). Pancreatic carcinoma cells induce fibrosis by stimulating proliferation and matrix synthesis of stellate cells. *Gastroenterology*, *128*(4), 907-921. doi:10.1053/j.gastro.2004.12.036
- Bhatia, R., Hill Michael, D., Shobha, N., Menon, B., Bal, S., Kochar, P., . . . Demchuk Andrew, M. (2010). Low Rates of Acute Recanalization With Intravenous Recombinant Tissue Plasminogen Activator in Ischemic Stroke. *Stroke*, *41*(10), 2254-2258. doi:10.1161/STROKEAHA.110.592535
- Bondy, C., Cheng, C., Zhong, J., & Lee, W. H. (2006). IGF-1 in Brain Growth and Repair Processes. In A. Lajtha & R. Lim (Eds.), *Handbook of Neurochemistry and Molecular Neurobiology: Neuroactive Proteins and Peptides* (pp. 143-165). Boston, MA: Springer US.
- Bonniaud, P., Margetts, P. J., Ask, K., Flanders, K., Gauldie, J., & Kolb, M. (2005). TGF-beta and Smad3 signaling link inflammation to chronic fibrogenesis. *J Immunol*, *175*(8), 5390-5395. doi:10.4049/jimmunol.175.8.5390
- Borthwick, L. A., & Wynn, T. A. (2015). IL-13 and TGF-β1: Core Mediators of Fibrosis. *Current Pathobiology Reports*, *3*(4), 273-282. doi:10.1007/s40139-015-0091-1
- Bouet, V., Boulouard, M., Toutain, J., Divoux, D., Bernaudin, M., Schumann-Bard, P., & Freret, T. (2009). The adhesive removal test: a sensitive method to assess sensorimotor deficits in mice. *Nature Protocols*, *4*(10), 1560-1564. doi:10.1038/nprot.2009.125
- Brainin, M., Feigin, V., Martins, S., Matz, K., Roy, J., Sandercock, P., . . . Wiseman, A. (2018). Cut stroke in half: Polypill for primary prevention in stroke. *International Journal of Stroke*, *13*(6), 633-647. doi:10.1177/1747493018761190
- Brait, V. H., Jackman, K. A., Walduck, A. K., Selemidis, S., Diep, H., Mast, A. E., . . . Sobey, C. G. (2010). Mechanisms contributing to cerebral infarct size after stroke: gender, reperfusion, T lymphocytes, and Nox2-derived superoxide. *Journal of cerebral blood flow and metabolism : official journal of the International Society of Cerebral Blood Flow and Metabolism*, *30*(7), 1306-1317. doi:10.1038/jcbfm.2010.14
- Buscemi, L., Price, M., Bezzi, P., & Hirt, L. (2019). Spatio-temporal overview of neuroinflammation in an experimental mouse stroke model. *Scientific Reports*, *9*(1), 507. doi:10.1038/s41598-018-36598-4

- Campbell, B. C. V., De Silva, D. A., Macleod, M. R., Coutts, S. B., Schwamm, L. H., Davis, S. M., & Donnan, G. A. (2019). Ischaemic stroke. *Nature Reviews Disease Primers*, 5(1), 70. doi:10.1038/s41572-019-0118-8
- Cano, E., Gebala, V., & Gerhardt, H. (2017). Pericytes or Mesenchymal Stem Cells: Is That the Question? *Cell Stem Cell*, 20(3), 296-297. doi:<https://doi.org/10.1016/j.stem.2017.02.005>
- Chung, A. G., Frye, J. B., Zbesko, J. C., Constantopoulos, E., Hayes, M., Figueroa, A. G., . . . Doyle, K. P. (2018). Liquefaction of the Brain following Stroke Shares a Similar Molecular and Morphological Profile with Atherosclerosis and Mediates Secondary Neurodegeneration in an Osteopontin-Dependent Mechanism. *eNeuro*, 5(5), ENEURO.0076-0018.2018. doi:10.1523/ENEURO.0076-18.2018
- Clarke, D. L., Carruthers, A. M., Mustelin, T., & Murray, L. A. (2013). Matrix regulation of idiopathic pulmonary fibrosis: the role of enzymes. *Fibrogenesis & tissue repair*, 6(1), 20-20. doi:10.1186/1755-1536-6-20
- Coutts, S. B. (2017). Diagnosis and Management of Transient Ischemic Attack. *Continuum (Minneapolis, Minn.)*, 23(1, Cerebrovascular Disease), 82-92. doi:10.1212/CON.0000000000000424
- Daneman, R., Zhou, L., Kebede, A. A., & Barres, B. A. (2010). Pericytes are required for blood-brain barrier integrity during embryogenesis. *Nature*, 468(7323), 562-566. doi:10.1038/nature09513
- Ding, S. (2014). Dynamic reactive astrocytes after focal ischemia. *Neural regeneration research*, 9(23), 2048-2052. doi:10.4103/1673-5374.147929
- Dirnagl, U., Iadecola, C., Moskowitz, M. A., Dirnagl, U., Iadecola, C., & Moskowitz, M. A. (1999). Pathobiology of ischaemic stroke: an integrated view. *Trends in Neurosciences*, 22(9). doi:OI:[https://doi.org/10.1016/S0166-2236\(99\)01401-0](https://doi.org/10.1016/S0166-2236(99)01401-0)
- Dorrier, C. E., Aran, D., Haenelt, E. A., Sheehy, R. N., Hoi, K. K., Pintarić, L., . . . Daneman, R. (2021). CNS fibroblasts form a fibrotic scar in response to immune cell infiltration. *Nature neuroscience*, 24(2), 234-244. doi:10.1038/s41593-020-00770-9
- Esposito, E., Li, W., Mandeville, E., Park, J., Şencan, I., Guo, S., . . . Lo, E. (2020). Potential circadian effects on translational failure for neuroprotection. *Nature*, 582. doi:10.1038/s41586-020-2348-z
- Everts, V., van der Zee, E., Creemers, L., & Beertsen, W. (1996). Phagocytosis and intracellular digestion of collagen, its role in turnover and remodelling. *The Histochemical journal*, 28(4), 229-245.
- Feng, Y., Liao, S., Wei, C., Jia, D., Wood, K., Liu, Q., . . . Jin, W.-N. (2017). Infiltration and persistence of lymphocytes during late-stage cerebral ischemia in middle cerebral artery occlusion and photothrombotic stroke models. *Journal of Neuroinflammation*, 14(1), 248. doi:10.1186/s12974-017-1017-0
- Fernández-Klett, F., & Priller, J. (2014). The Fibrotic Scar in Neurological Disorders. *Brain Pathology*, 24(4), 404-413. doi:<https://doi.org/10.1111/bpa.12162>
- G. Gabbiani, A. O. (2006). Encyclopedia of Respiratory Medicine.

- García-Cabezas, M. Á., John, Y. J., Barbas, H., & Zikopoulos, B. (2016). Distinction of Neurons, Glia and Endothelial Cells in the Cerebral Cortex: An Algorithm Based on Cytological Features. *Frontiers in neuroanatomy*, *10*, 107-107. doi:10.3389/fnana.2016.00107
- Goldschmidt, R. C., Hough, L. B., & Glick, S. D. (1985). Rat brain mast cells: contribution to brain histamine levels. *J Neurochem*, *44*(6), 1943-1947. doi:10.1111/j.1471-4159.1985.tb07191.x
- Göritz, C., Dias, D., Tomilin, N., Barbacid, M., Shupliakov, O., & Frisén, J. (2011a). A Pericyte Origin of Spinal Cord Scar Tissue. *Science (New York, N.Y.)*, *333*, 238-242. doi:10.1126/science.1203165
- Göritz, C., Dias, D. O., Tomilin, N., Barbacid, M., Shupliakov, O., & Frisén, J. (2011b). A Pericyte Origin of Spinal Cord Scar Tissue. *Science*, *333*(6039), 238. doi:10.1126/science.1203165
- Grefkes, C., & Fink, G. R. (2020). Recovery from stroke: current concepts and future perspectives. *Neurological Research and Practice*, *2*(1), 17. doi:10.1186/s42466-020-00060-6
- Hamill, K. J., Kligys, K., Hopkinson, S. B., & Jones, J. C. R. (2009). Laminin deposition in the extracellular matrix: a complex picture emerges. *Journal of Cell Science*, *122*(24), 4409. doi:10.1242/jcs.041095
- Hari Garg, C. H. (2004). *Chemistry and Biology of Hyaluronan*
1st Edition.
- Hu, D., Yin, C., Luo, S., Habenicht, A. J. R., & Mohanta, S. K. (2019). Vascular Smooth Muscle Cells Contribute to Atherosclerosis Immunity. *Frontiers in Immunology*, *10*(1101). doi:10.3389/fimmu.2019.01101
- Hurford, R., Sekhar, A., Hughes, T. A. T., & Muir, K. W. (2020). Diagnosis and management of acute ischaemic stroke. *Practical Neurology*, *20*(4), 304. doi:10.1136/practneurol-2020-002557
- Hynes, R. O., & Naba, A. (2012). Overview of the matrisome--an inventory of extracellular matrix constituents and functions. *Cold Spring Harb Perspect Biol*, *4*(1), a004903. doi:10.1101/cshperspect.a004903
- Jayaraj, R. L., Azimullah, S., Beiram, R., Jalal, F. Y., & Rosenberg, G. A. (2019). Neuroinflammation: friend and foe for ischemic stroke. *Journal of Neuroinflammation*, *16*(1), 142. doi:10.1186/s12974-019-1516-2
- Jovin Tudor, G., Albers Gregory, W., Liebeskind David, S., & null, n. (2016). Stroke Treatment Academic Industry Roundtable. *Stroke*, *47*(10), 2656-2665. doi:10.1161/STROKEAHA.116.013578
- Kelly, K. K., MacPherson, A. M., Grewal, H., Strnad, F., Jones, J. W., Yu, J., . . . Siegenthaler, J. A. (2016). Col1a1+ perivascular cells in the brain are a source of retinoic acid following stroke. *BMC Neurosci*, *17*(1), 49. doi:10.1186/s12868-016-0284-5
- Kendall, R. T., & Feghali-Bostwick, C. A. (2014). Fibroblasts in fibrosis: novel roles and mediators. *Frontiers in Pharmacology*, *5*(123). doi:10.3389/fphar.2014.00123

- Kinnula, V. L., Fattman, C. L., Tan, R. J., & Oury, T. D. (2005). Oxidative stress in pulmonary fibrosis: a possible role for redox modulatory therapy. *Am J Respir Crit Care Med*, 172(4), 417-422. doi:10.1164/rccm.200501-017PP
- Kisseleva, T., & Brenner, D. A. (2008). Mechanisms of fibrogenesis. *Exp Biol Med (Maywood)*, 233(2), 109-122. doi:10.3181/0707-mr-190
- Lakhan, S., Kirchgessner, A., & Hofer, M. (2009). Lakhan SE, Kirchgessner A, Hofer M Inflammatory mechanisms in ischemic stroke: therapeutic approaches. *J Transl Med* 7:97. *Journal of translational medicine*, 7, 97. doi:10.1186/1479-5876-7-97
- Lam, M. A., Hemley, S. J., Najafi, E., Vella, N. G. F., Bilston, L. E., & Stoodley, M. A. (2017). The ultrastructure of spinal cord perivascular spaces: Implications for the circulation of cerebrospinal fluid. *Scientific Reports*, 7(1), 12924. doi:10.1038/s41598-017-13455-4
- Lewitt, M. S., & Boyd, G. W. (2019). The Role of Insulin-Like Growth Factors and Insulin-Like Growth Factor-Binding Proteins in the Nervous System. *Biochemistry insights*, 12, 1178626419842176-1178626419842176. doi:10.1177/1178626419842176
- Li, X., Li, M., Tian, L., Chen, J., Liu, R., & Ning, B. (2020). Reactive Astrogliosis: Implications in Spinal Cord Injury Progression and Therapy. *Oxidative Medicine and Cellular Longevity*, 2020, 9494352. doi:10.1155/2020/9494352
- Liu, R., Pan, M.-X., Tang, J.-C., Zhang, Y., Liao, H.-B., Zhuang, Y., . . . Wan, Q. (2017). Role of neuroinflammation in ischemic stroke. *Neuroimmunology and Neuroinflammation*, 4, 158-166. doi:10.20517/2347-8659.2017.09
- Liu, Z., & Chopp, M. (2016). Astrocytes, therapeutic targets for neuroprotection and neurorestoration in ischemic stroke. *Progress in neurobiology*, 144, 103-120. doi:10.1016/j.pneurobio.2015.09.008
- Lodish, H., Berk, A., Zipursky, S. L., Matsudaira, P., Baltimore, D., & Darnell, J. (2000). Collagen: the fibrous proteins of the matrix. *Molecular cell biology*, 4.
- Mescher, A. L. (2017). Macrophages and fibroblasts during inflammation and tissue repair in models of organ regeneration. *Regeneration (Oxford, England)*, 4(2), 39-53. doi:10.1002/reg2.77
- Mithieux, S. M., & Weiss, A. S. (2005). Elastin. *Advances in protein chemistry*, 70, 437-461.
- Moreno-García, A., Kun, A., Calero, O., Medina, M., & Calero, M. (2018). An Overview of the Role of Lipofuscin in Age-Related Neurodegeneration. *Frontiers in neuroscience*, 12, 464-464. doi:10.3389/fnins.2018.00464
- Morizawa, Y. M., Hirayama, Y., Ohno, N., Shibata, S., Shigetomi, E., Sui, Y., . . . Koizumi, S. (2017). Reactive astrocytes function as phagocytes after brain ischemia via ABCA1-mediated pathway. *Nature Communications*, 8(1), 28. doi:10.1038/s41467-017-00037-1
- Mu, X., Bellayr, I., Walters, T., & Li, Y. (2010). Mediators leading to fibrosis - how to measure and control them in tissue engineering. *Operative techniques in orthopaedics*, 20(2), 110-118. doi:10.1053/j.oto.2009.10.003

- Munji, R. N., Soung, A. L., Weiner, G. A., Sohet, F., Semple, B. D., Trivedi, A., . . . Daneman, R. (2019). Profiling the mouse brain endothelial transcriptome in health and disease models reveals a core blood-brain barrier dysfunction module. *Nature neuroscience*, 22(11), 1892-1902. doi:10.1038/s41593-019-0497-x
- Musuka, T. D., Wilton, S. B., Traboulsi, M., & Hill, M. D. (2015). Diagnosis and management of acute ischemic stroke: speed is critical. *CMAJ : Canadian Medical Association journal = journal de l'Association medicale canadienne*, 187(12), 887-893. doi:10.1503/cmaj.140355
- O'Sullivan, C., Weible, A. P., & Wehr, M. (2019). Auditory Cortex Contributes to Discrimination of Pure Tones. *eNeuro*, 6(5), ENEURO.0340-0319.2019. doi:10.1523/ENEURO.0340-19.2019
- Parmar, P. (2015). Stroke: Treatment options in acute management. *Pharmaceutical Journal*, 294, 562-566.
- Parrella, E., Porrini, V., Benarese, M., & Pizzi, M. (2019). The Role of Mast Cells in Stroke. *Cells*, 8(5), 437. doi:10.3390/cells8050437
- Rajkumar, V. S., Shiwen, X., Bostrom, M., Leoni, P., Muddle, J., Ivarsson, M., . . . Abraham, D. J. (2006). Platelet-derived growth factor-beta receptor activation is essential for fibroblast and pericyte recruitment during cutaneous wound healing. *The American journal of pathology*, 169(6), 2254-2265. doi:10.2353/ajpath.2006.060196
- Rangaraju, S., Raza, S. A., Li, N. X. A., Betarbet, R., Dammer, E. B., Duong, D., . . . Levey, A. I. (2018). Differential Phagocytic Properties of CD45^{low} Microglia and CD45^{high} Brain Mononuclear Phagocytes—Activation and Age-Related Effects. *Frontiers in Immunology*, 9(405). doi:10.3389/fimmu.2018.00405
- Roth, M., Enström, A., Aghabeick, C., Carlsson, R., Genové, G., & Paul, G. (2020). Parenchymal pericytes are not the major contributor of extracellular matrix in the fibrotic scar after stroke in male mice. *Journal of neuroscience research*, 98(5), 826-842. doi:10.1002/jnr.24557
- Sayed, M. A., Eldahshan, W., Abdelbary, M., Pillai, B., Althomali, W., Johnson, M. H., . . . Fagan, S. C. (2020). Stroke promotes the development of brain atrophy and delayed cell death in hypertensive rats. *Scientific Reports*, 10(1), 20233. doi:10.1038/s41598-020-75450-6
- Schnell, S. A., Staines, W. A., & Wessendorf, M. W. (1999). Reduction of Lipofuscin-like Autofluorescence in Fluorescently Labeled Tissue. *Journal of Histochemistry & Cytochemistry*, 47(6), 719-730. doi:10.1177/002215549904700601
- Schuppan, D., Ruehl, M., Somasundaram, R., & Hahn, E. G. (2001). Matrix as a modulator of hepatic fibrogenesis. *Semin Liver Dis*, 21(3), 351-372. doi:10.1055/s-2001-17556
- Shibahara, T., Ago, T., Nakamura, K., Tachibana, M., Yoshikawa, Y., Komori, M., . . . Kitazono, T. (2020). Pericyte-Mediated Tissue Repair through PDGFR β Promotes Peri-Infarct Astroglia, Oligodendrogenesis, and Functional Recovery after Acute Ischemic Stroke. *eNeuro*, 7(2), ENEURO.0474-0419.2020. doi:10.1523/ENEURO.0474-19.2020

- Shiotsuki, H., Yoshimi, K., Shimo, Y., Funayama, M., Takamatsu, Y., Ikeda, K., . . . Hattori, N. (2010). A rotarod test for evaluation of motor skill learning. *J Neurosci Methods*, *189*(2), 180-185. doi:10.1016/j.jneumeth.2010.03.026
- Silverman, A.-J., Sutherland, A. K., Wilhelm, M., & Silver, R. (2000). Mast Cells Migrate from Blood to Brain. *The Journal of Neuroscience*, *20*(1), 401. doi:10.1523/JNEUROSCI.20-01-00401.2000
- Suryadevara, V., Ramchandran, R., Kamp, D. W., & Natarajan, V. (2020). Lipid Mediators Regulate Pulmonary Fibrosis: Potential Mechanisms and Signaling Pathways. *International Journal of Molecular Sciences*, *21*(12). doi:10.3390/ijms21124257
- Sziksz, E., Pap, D., Lippai, R., Béres, N. J., Fekete, A., Szabó, A. J., & Vannay, Á. (2015). Fibrosis Related Inflammatory Mediators: Role of the IL-10 Cytokine Family. *Mediators of Inflammation*, *2015*, 764641. doi:10.1155/2015/764641
- Tennant, K. A., Asay, A. L., Allred, R. P., Ozburn, A. R., Kleim, J. A., & Jones, T. A. (2010). The vermicelli and capellini handling tests: simple quantitative measures of dexterous forepaw function in rats and mice. *Journal of visualized experiments : JoVE*(41), 2076. doi:10.3791/2076
- Tidball, J. G. (2005). Inflammatory processes in muscle injury and repair. *Am J Physiol Regul Integr Comp Physiol*, *288*(2), R345-353. doi:10.1152/ajpregu.00454.2004
- Unnithan AKA, M. P. (2020). Hemorrhagic Stroke. *StatPearls* Retrieved from <https://www.ncbi.nlm.nih.gov/books/NBK559173/>
- van Caam, A., Vonk, M., van den Hoogen, F., van Lent, P., & van der Kraan, P. (2018). Unraveling SSc Pathophysiology; The Myofibroblast. *Frontiers in Immunology*, *9*(2452). doi:10.3389/fimmu.2018.02452
- Van Vliet, E., Melis, M., Foidart, J. M., & Van Ewijk, W. (1986). Reticular fibroblasts in peripheral lymphoid organs identified by a monoclonal antibody. *Journal of Histochemistry & Cytochemistry*, *34*(7), 883-890. doi:10.1177/34.7.3519751
- Vanlandewijck, M. (2018). A molecular atlas of cell types and zonation in the brain vasculature. *Nature*, *554*. Retrieved from <http://betsholtzlab.org/VascularSingleCells/database.htm>
- Wynn, T. A. (2008). Cellular and molecular mechanisms of fibrosis. *J Pathol*, *214*(2), 199-210. doi:10.1002/path.2277
- Xue, M., & Jackson, C. (2013). Extracellular Matrix Reorganization During Wound Healing and Its Impact on Abnormal Scarring. *Advances in Wound Care*, *4*, 131106055742000. doi:10.1089/wound.2013.0485
- Yue, B. (2014). Biology of the extracellular matrix: an overview. *Journal of glaucoma*, *23*(8 Suppl 1), S20-S23. doi:10.1097/IJG.0000000000000108
- Zerna, C., Hill Michael, D., & Boltze, J. (2017). Towards Improved Translational Stroke Research. *Stroke*, *48*(9), 2341-2342. doi:10.1161/STROKEAHA.117.017906

6. Acknowledgments

I would like to thank and acknowledge the following people and institutions without whom my project would not have been possible nor deductible:

Dr. Richard Daneman for all the guidance, advice and encouragement throughout the entire project. For believing in me and supporting me in all of the challenges 2020/2021 had to offer as well as in my future career. Your constant care and advice have not only helped me become a better scientist, but a better person as well.

To my **fellow researchers** at the Daneman lab, for creating the most positive, fun and knowledgeable environment I have ever encountered in science. You have all made me feel like I was home, while I was 10000 miles away from it. Thank you for all the love and support during lab hours and in our non-working times. Additionally, thank you for every sacrifice you have made with your own time and experiments, so that I can finish my project. Furthermore, I want to extend a very special thank you to Iris Garcia-Pak and **Dr. Cayce Dorrier**. I cannot express my gratitude to Dr. Dorrier for being my mentor and teaching me all of the necessary skills and techniques needed for my research and future career. And **Ms. Garcia-Pak**, who selflessly helped me during raw data collection to ensure I manage to perform all of the experiments. Also, for all of the subsequent revision experiments you have been a part of.

I would also like to thank my internal supervisor, **Prof. Swoboda** for all her help during my time away and with the master thesis. Moreover, I want to thank University of Applied Sciences FH Krems an der Donau and FH Campus Wien who provided me with quality education to be able to pursue and contribute to scientific discoveries.

Furthermore, this project would have not been possible without the financial support of the **Austrian Marshall Plan Foundation**. I feel very honored to be called a Marshall Plan Foundation recipient.

Finally, and most importantly, I want to thank my **family**. Mom – thank you for being the most admirable, strong, loving and inspirational women I have ever met. You have showed me what love is and how to display it. Dad, thank you for working so hard to give me and my brother the best education and opportunities in life you could. Your internal drive, loyalty, integrity and ‘never-give-up’ attitude is what shaped me into the woman you see today. Even though both of you were absolutely terrified of every step I took further away from you in the last 6 years, you have emotionally and financially supported me every step of the way. You have always put my happiness in front of yours. Thank you from the bottom of my heart. Lastly, to my older brother Jasminko. Thank you for showing me what hard work is and for supporting me in all of my accomplishments. I am so proud of what you have achieved thus far and how you always have fun along the way. You have always kept me grounded and/or frustrated as a brother should. I love you.

7. Statutory Declaration

Erklärung:

Ich erkläre, dass die vorliegende Diplomarbeit/Masterarbeit von mir selbst verfasst wurde und ich keine anderen als die angeführten Behelfe verwendet bzw. mich auch sonst keiner unerlaubter Hilfe bedient habe.

Ich versichere, dass ich diese Diplomarbeit/Masterarbeit bisher weder im In- noch im Ausland (einer Beurteilerin/einem Beurteiler zur Begutachtung) in irgendeiner Form als Prüfungsarbeit vorgelegt habe.

Weiters versichere ich, dass die von mir eingereichten Exemplare (ausgedruckt und elektronisch) identisch sind.

Declaration:

I hereby declare that the submitted Master thesis was written by myself and that I did not use any aids other than those indicated, none of which are unauthorised.

I assure that I have not previously submitted this Master thesis or its contents in any form for assessment as part of an examination either in Austria or abroad.

Furthermore, I assure that all copies submitted by myself (electronic and printed) are identical.

date: 18.02.2021.....

signature: 